Susana Filipe Ferreira

Licenciada em Biologia

Optimization of Neoadjuvant Radiotherapy for zebrafish-avatars - towards personalized medicine

Dissertação para obtenção do Grau de Mestre em

Genética Molecular e Biomedicina

Orientadora: Dra. Rita Fior, PhD

FACULDADE DE CIÊNCIAS E TECNOLOGIA
UNIVERSIDADE NOVA DE LISBOA

Susana Filipe Ferreira

Licenciada em Biologia

Optimization of Neoadjuvant Radiotherapy for zebrafish-avatars - towards personalized medicine

Dissertação para obtenção do Grau de Mestre em

Genética Molecular e Biomedicina

Orientadora: Dra. Rita Fior, PhD

Trabalho experimental desenvolvido na

Fundação Champalimaud – Champalimaud Centre for the Unknown

Setembro, 2018

Optimization of Neoadjuvant Radiotherapy for zebrafish-avatars - towards personalized medicine

Acknowledgments

Gostaria de deixar um agradecimento sincero a todos aqueles que me acompanharam durante este fantástico percurso:

Em primeiro lugar, gostaria de agradecer à Doutora Rita Fior e ao Doutor Miguel Godinho por me terem dado a oportunidade de poder desenvolver o projeto de Mestrado no vosso laboratório. Obrigada por me ajudarem a crescer e me mostrarem o quão fascinante a ciência e a investigação consegue ser.

Rita, quero-lhe agradecer por me ter acompanhado de forma persistente neste desafio como minha orientadora. Graças aos seus ensinamentos, conselhos e "dicas", desafiei-me a mim própria, aprendi, cresci e adquiri experiência. Muito obrigada pela sua total disponibilidade, por me ensinar a enfrentar os desafios sempre com uma atitude positiva, aberta e pensar de uma forma crítica para além daquilo que vemos e que nos é dado como garantido. Obrigada por me ajudar e ensinar a descomplicar o meu complicado: "Keep it simple, Susana!". Muito obrigada pelo apoio, ajuda e boa disposição. Levarei comigo com muito carinho tudo o que aprendi consigo, muito obrigada!

Miguel, muito obrigada pelas discussões científicas, por me incentivar a pensar criticamente sobre os problemas e de como os podemos solucionar. Obrigada uma vez mais por fazer parte do meu processo de aprendizagem, por me "educar cientificamente" usando o raciocínio científico e por partilhar o gosto pela ciência e curiosidade pelo desconhecido. Muito obrigada!

Bruna, obrigada por me teres acompanhado durante esta minha caminhada, pelos conselhos sábios, pelo apoio incondicional, ajuda, paciência, mas acima de tudo pela amizade. Foste fundamental para o desenvolvimento deste trabalho, para o meu crescimento e independência no laboratório, e estou-te muito grata por isso! Obrigada pela disponibilidade e a boa disposição com que sempre me ajudaste. Muito obrigada Bruna!

Vanda, esse brilho no teu olhar e gosto pela ciência é cativante! Obrigada por partilhares comigo os teus conhecimentos, pelos ensinamentos e pela ajuda incessante que me deste. Obrigada pelas discussões críticas e entusiasmantes e acima de tudo por me apoiares e incentivares a nunca desistir.

Raquel, muito obrigada pela disponibilidade, ajuda e amizade. Quero também agradecer à Magda pela compreensão, interajuda e apoio incondicional que me deu ao longo deste percurso. Foste um grande exemplo para mim, pela persistência com que demonstraste que nunca se desiste dos sonhos, obrigada! Mariana e Andreia obrigada por fazerem parte desta minha jornada e por se me mostrarem sempre disponíveis.

Cátia, a minha grande companheira desta jornada fantástica, obrigada por tudo! Obrigada pelo apoio, ajuda e pela amizade sincera. Foi um prazer partilhar contigo esta caminhada. Guardarei com muito carinho todos os momentos divertidos e de trabalho que partilhámos. Muito obrigada!

Quero também agradecer a toda a equipa do departamento de Radioterapia – Dr.Oriol Parés, Dra. Sandra Vieira e Maria João Cardoso – e da Fish Facility – Joana, Rita e Carolina – pela disponibilidade, ajuda e boa disposição!

Finalmente, gostaria de agradecer à minha família que foram determinantes neste meu percurso. Quero agradecer especialmente aos meus pais, Paulo e Rosa e ao meu namorado Bruno por me apoiarem incondicionalmente e pela extrema paciência que tiveram. Sem vocês nada disto seria possível, um sincero obrigado!

Gostaria de terminar por dedicar este trabalho ao meu avô Ferreira, que nunca desistiu de lutar e que sempre foi um exemplo que com trabalho e dedicação conseguimos alcançar os nossos objetivos.

Espero que todo o esforço e dedicação desta equipa maravilhosa consiga alcançar os seus objetivos, e que o nosso peixinho-zebra possa vir a contribuir e a marcar a diferença na vida de muitas pessoas! Muito obrigada a todos!

Resumo

Recentemente o Laboratório Telómeros e Cancro (Fundação Champalimaud) desenvolveu um modelo de xenografos em peixe-zebra de cancro colo-rectal, que permite discriminar diferentes sensibilidades à Quimioterapia Adjuvante recomendada na clínica (Fior *et al*., 2017). Atualmente, o objetivo do Laboratório consiste em testar se este modelo permite também discriminar diferentes sensibilidades à Radioterapia Neoadjuvante. O regime Neoadjuvante recomendado como tratamento para o combate ao cancro rectal consiste numa Radioterapia Fracionada (5x5Gy), tendo como objetivo a diminuição do tamanho tumoral antes de submetido a cirurgia. Resultados preliminares (Póvoa e Fior) demonstraram que xenografos de peixe-zebra têm a capacidade de diferenciar tumores radiossensíveis de radioresistentes, usando um protocolo adaptado de dose única (1x25Gy) diferente do usado na clínica (5x5Gy). Assim, questionou-se se o regime adaptado (1x25Gy) seria suficiente aproximação, de modo a ser usado como uma estimativa da resposta do tumor à radiação terapêutica de 5x5Gy.

Deste modo, o principal objetivo deste trabalho consistiu na comparação dos dois protocolos de Radioterapia: (1x25Gy) *versus* (5x5Gy). Para tal, células de cancro colo-rectal radiossensíveis foram injetadas em peixe-zebra, sendo estes sujeitos às seguintes condições experimentais: Controlo; 5x5Gy, e 1x25Gy. Os nossos resultados revelaram que ao sexto dia após-injeção, o regime 1x25Gy consegue desencadear respostas tumorais semelhantes à Radioterapia Fracionada. Assim, o regime 1x25Gy parece ser suficiente para um rápido e exequível ensaio. Porém, ao avaliar a relevância do factor "tempo" pós-radiação, os resultados sugerem que danos acumulativos e tempo são fatores cruciais para uma resposta anti-tumoral mais eficaz. Ainda assim, o regime de dose única (1x25Gy) parece ser adequado para o acesso rápido da resposta tumoral, contudo é necessário testar células radioresistentes. Adicionalmente, durante este trabalho foram desenvolvidos avatares peixe-zebra de cancro colo-rectal, os quais foram submetidos a tratamentos de Radioterapia e Radio-Quimioterapia, observando-se um aumento de morte celular no regime combinatório.

Palavras-chave: Cancro colo-rectal, Radioterapia, Dose única (1x25Gy), Doses fracionadas (5x5Gy), Radiosensibilidade

Abstract

Recently, Fior and colleagues developed zebrafish Patient-derived Xenografts (zPDX) for personalized medicine to quickly screen the recommended Adjuvant Chemotherapies for colorectal cancer (CRC). Now the Lab goal is to test if zPDX can also be used to screen patients for Neoadjuvant Radiotherapy (RT). In rectal cancer the Neoadjuvant RT comprises a short Fractionated RT regimen of 5x5Gy (FRT), used to shrink tumor before surgery. Preliminary results from the Lab showed to be possible to distinguish radiosensitive from radioresistant CRC zebrafish xenografts, using an adapted RT protocol Single-High Dose RT (SHD-RT, 1x25Gy). However this SHD-RT protocol was different from the one given in the clinic (FRT, 5x5Gy), raising the question whether this adaptation is a good proxy of tumor response. Thus, the main goal of this thesis was to compare both RT protocols and test if SHD-RT is suitable to determine tumor radiosensitivity/radioresistance. To address this aim, radiosensitive CRC zebrafish xenografts were generated and distributed into the different experimental conditions: Control (non-irradiated); FRT; and SHD-RT. Our results revealed that SHD-RT induces similar tumor responses to FRT, in 6 days, i.e. both protocols lead to a significant induction of apoptosis and reduction of tumor size, suggesting that SHD-RT is enough for a quick and feasible assay. However, we also investigated further the cumulative effect of radiation and whether "time matters" for the radiobiology of the tumors in this short assay. Indeed, our results showed that cumulative damage and time are crucial factors to reduce the overall tumor size. However, given the similar results in the 6dpi assay, the adapted SHD-RT protocol seemed a practical option for the zPDX assay. Nevertheless this study needs further confirmation with a radioresistant tumor. Moreover, CRC zebrafish avatars were tested for RT and its combination with Chemotherapy, suggesting an increase of apoptotic cells upon the treatment combination.

Keywords: Colorectal cancer, Radiotherapy, SHD-RT, FRT, Zebrafish xenografts, Radiosensitivity

Contents

Figures contents

Figure 5.2. Growth rate of CRC HCT116 cells in zebrafish. The values in A are the overall results obtained from the quantification of the tumor size from all non-irradiated controls xenografts along the RT experiments. Thus, it was possible to analyze HCT116 cells proliferation in zebrafish through time. Regarding the DAPI numbers, HCT116 showed to double the size in 4 days: 2dpi AVG=1538,74; 4dpi AVG=2059,53; 6dpi AVG= 3151,34; 8dpi AVG=4239,08. For the results in Figure 3.8 it was estimated that the tumor size at 5dpi had an average of ~ 2900 cells. Given that HCT116 cells doubled de size in 4 days, it was estimated that at 1dpi the tumor size should exhibited an average of ~1450 cells, i.e. from day 1 to day 5, the CRC cells increased the double. 50

Tables contents

Abbreviations

act.Caspase3 – activated Caspase3
APC – Adenomatous Polyposis Coli gene
ATM – Ataxia Telangiectasia mutated (kinase)
ATR – AT-related (kinase)
AVG – Average
CEA – Carcinoembryonic Antigen
CIN – Chromosomal Instability
ChT – Chemotherapy
CRC – Colorectal cancer
CRT – Chemoradiotherapy
DAPI – 4',6-Diamidino-2-Phenylindole
DFS – Disease-Free Survival
DMEM – Dulbecco's Modified Eagle Medium
DMSO – Dimethyl Sulfoxide
DNA-PK – DNA-dependent Protein Kinase
DPBS – Dulbecco's Phosphate-Buffered Saline
DSB – Double-Strand Break
dpT – days-post treatment
dpf – days-post fertilization
dpi – days-post injection
E3 – Embryo medium
eGFP – Enhanced Green Fluorescent Protein
FBS – Fetal Bovine Serum
FRT – Fractionated Radiotherapy
FA – Formaldehyde
Gy – Gray
hpr – hours-post radiation
hpi – hours-post injection
hmito – Human mitochondria
HR – Homologous Recombination
IR – Ionizing Radiation
LET – Low Linear Energy Transfer
Mac – Macrophages
MeOH – Methanol
N – Number of samples
NA – Neoadjuvant
NHEJ – Non-Homologous End Joining
ns – Nonsignificant (statistical analysis)
NSCLC – Non-Small-Cell Lung Cancer
P – *P value*
PBS – Phosphate Buffered Saline
PVS – Perivitelline Space
RT – Radiotherapy

RNS – Reactive Nitrogen Species
ROS – Reactive Oxygen Species
SABR – Stereotactic Ablative Radiotherapy
SBRT – Stereotactic Body Radiation Therapy
SCPRT – Short-Course Perioperative Radiotherapy
SD – Standard Deviation
SHD-RT – Single-High Dose Radiotherapy
SSB – Single-Strand Break
TAMs – Tumor-associated Macrophages
TME – Tumor Microenvironment
TNFα – Tumor Necrosis Factor Alpha
5-FU –5-Fluorouracil (fluoropyrimidine)
zPDX – Zebrafish Patient-derived Xenografts

1. Introduction

1.1 Cancer

Multicellular organisms are developed and maintained under highly controlled and precise rules, where each cell behaves for the organism homeostasis. However, cancer cells can break and escape the rules that maintains a healthy organism. Both genetic and environmental factors play an important role in cancer development, known as a multifactorial disease. The acquisition of several mutations may give cells a selective advantage, which drives to malignant cancer transformation with uncontrolled proliferation capacity, invading the surrounding tissues, metastasizing and colonizing distant sites through blood circulation (Alberts *et al*., 2002). The successive changes gives cancer cells capabilities, named "hallmarks of cancer", that allow tumor growth and further metastatic dissemination (Hanahan and Weinberg, 2011), such as:

1. Sustained proliferation by deregulation of growth signals;
2. Ability to resist to cell death through several mechanisms and strategies to escape apoptosis;
3. Replicative immortality, maintaining DNA length by preventing telomeres shortening to avoid apoptosis and senescence;
4. Invasion and metastasis activation through epithelial-mesenchymal transition, where cells are able to invade, resist to apoptosis and disseminate;
5. Promotion of angiogenesis to sustain tumor viability and progression;
6. Immune system evasion – development of mechanisms to escape immune recognition or by inducing immune suppression;
7. Reprogrammed energy metabolism (aerobic glycolysis, where even in the presence of oxygen, cancer cells promote glucose metabolism instead of oxidative phosphorylation – Warburg phenomenon);

Beside the acquisition of several somatic mutations, cancer can also be driven by epigenetic alterations, a consequence of changes in the chromatin structure without affecting DNA sequence which ultimately results in modifications of gene expression. DNA methylation, histone modifications and non-coding RNA are epigenetic factors that can lead to oncogene activation or tumor suppressor loss of function, triggering tumorigenesis (Alberts *et al*., 2002). The tumor microenvironment (TME) is also an essential factor in cancer development and progression, composed by connective tissue, cancer-associated fibroblasts, endothelial cells, pericytes, cancer stem cells, immune inflammatory cells and extracellular matrix. The dynamic communication between tumor and TME, such as intercellular interactions mediated by several signals (growth factors, enzymes, and cytokines) is fundamental for tumor growth and fate (Balkwill *et al*., 2012).

1.1.1 Colorectal cancer

Colorectal cancer (CRC) is the second most commonly diagnosed cancer in Europe and a worldwide leading cause of death (Cutsem *et al*., 2016). Defined as a carcinoma with origin in the

epithelium lining the colon (large intestine) and rectum (gut terminal segment), CRC is one of the most predominant cancers, influenced by the extremely fast rate of cell proliferation and turnover that occurs in the epithelial tissue, in adults. Stem cells and intestinal crypts (deep epithelium pockets) signals are responsible for the control of normal organization of the epithelium tissue dictating its renewal. Nevertheless, the arising of mutations can disrupt these signals, leading to tumor formation. A protruding mass, called polyp (adenoma), is formed and it can grow through time, arising abnormal and mutated cells in non-organized structures. Cancer cells can become invasive, disrupting the epithelial basal lamina and consequently migrate to the surrounding tissues (Alberts *et al*., 2002).

Environmental and genetic factors play an important role in CRC development. The accumulation of somatic mutations in response to the environment is the major cause of CRC, named "sporadic" or non-heritable CRC (Kuipers *et al*., 2015). Many genes and pathways are affected leading to genomic instability, with highlight: 1) the adenomatous polyposis coli (*APC*) tumor suppressor gene, which controls the activity of the WNT signalling pathway; 2) proto-oncogene *K-Ras* (member of *Ras* gene family); 3) the tumor suppressor involved in stress responses and DNA damage, *p53* gene; 4) and the Chromosomal Instability (CIN) pathway, that leads to chromosomal abnormalities. The heritable component is another leading factor for CRC development, more pronounced for colon than rectal cancer (Glynne-Jones *et al*., 2017). The most commonly hereditary CRC syndromes are Familial Adenomatous Polyposis (FAP) and Lynch syndromes that results of genetic mutations in *APC* gene and DNA mismatch-repair genes, respectively, associated with an increased risk of CRC incidence (Alberts *et al*., 2002). Beside the genetic component, lifestyle is also a determinant environmental factor that influences the risk of developing CRC, increasing with smoking, alcohol, dietary habits, as red meet ingestion and obesity. Additionally to polyp formation, the tumor microenvironment, such as the gut microbiota and the tissue inflammatory dynamics, can modulate cancer, leading to mutations and consequently tumor progression. Thus, CRC leading causes are responsible to generate both genetic mutations and epigenetic modifications that progressively induce cell transformation, following clonal expansion and selection of those who have a biological fitness advantage to disseminate through the organism (Kuipers *et al*., 2015).

1.1.2 Colorectal cancer therapeutic options

Colon cancer and rectal cancer are distinct tumors, classified as >15cm and ≤ 15cm distal extensions from the anal margin, respectively. Curative surgery is the mainstay for CRC treatment, however, according to the tumor stage, colon and rectal cancer have different approaches and managements (Briffa *et al*., 2018). Regarding colon cancer, Adjuvant Chemotherapy (ChT) is recommended to prevent distant metastasis following curative resection, with prolonged survival. Adjuvant ChT is considered the standard treatment for patients with "high-risk" stage II and stage III colon cancer where FOLFOX (a combination of 5-FU (fluoropyrimidine 5-fluorouracil) with oxaliplatin and folinic acid (leucovorin)), is given (Glynne-Jones *et al*., 2017). 5-FU can be delivered in monotherapy, which is incorporated in DNA and RNA as well inhibits essential biosynthetic processes,

leading to genomic dysfunction (Longley *et al*., 2003). The addition of oxaliplatin, responsible for the blockade of DNA replication and transcription (Seetharam *et al*., 2010), seems to improve disease-free survival (DFS) (Glynne-Jones *et al*., 2017), whereas folinic acid potentiates the inhibitory effect of 5-FU (Erlichman *et al*., 1988). Regarding the meta-analysis performed for colon cancer treatment with FOLFOX revealed a response rate of 40%-50% (Wu *et al*., 2017a). Beside this intravenously combination, XELOX (oxaliplatin and capecitabine, an oral fluoropyrimide converted in 5-FU in the tumor site (Twelves *et al*., 2005)) can also be used in Adjuvant ChT for colon cancer as an oral approach (Kuipers *et al*., 2015) (Table 1.1). Adjuvant 5-FU-based ChT, in the absence of any preoperative therapy, can be also applied for rectal cancer, although the benefits are lower than for colon cancer.

The Neoadjuvant (NA) setting, performed prior to surgery, is the preferable approach for rectal cancer treatment. According to the clinical practice guidelines, Short-Course Preoperative Radiotherapy (SCPRT) or Chemoradiotherapy (CRT) are the routine treatments for intermediate stage or locally advanced rectal cancer, with the aim to reduce local recurrence and tumor downstaging (Glynne-Jones *et al*., 2017). SCPRT is based on the delivery of 5Gy irradiation for five consecutive days (5x5Gy), followed by surgery, while in conventional CRT radiation is delivered in 25-28 fractions with approximately 1.8 – 2Gy, totalizing 45-50Gy, with 5-FU-based ChT (Glynne-Jones *et al*., 2017; Okuyama *et al*., 2018). FOLFOX ChT following SCPRT is also frequent to improve the NA treatment (Table 1.1). 12 weeks after NA treatment, tumor response can be assessed, where is graded as: complete response (8-20%), partial response (40%) or no response to therapy (20%) (Dayde *et al*., 2017; Glynne-Jones *et al*., 2017). Either in colon or rectum anti-cancer approaches, carcinoembryonic antigen (CEA) serum levels, the most commonly tumor marker in CRC patients, are evaluated before treatment or surgery to provide a baseline value for post-treatment or -resection prognosis (Kim *et al*., 2017). Raised CEA (glycoprotein promotes cell adhesion allowing CRC cells aggregation) levels, approximately in 60-85% of CRC patients, are expected to return to normal values after therapy (< 5ng/ml) (Glynne-Jones *et al*., 2017; Stiksma *et al*., 2014). Carbohydrate 19-9 antigen (CA 19-9) is another biomarker for CRC prognosis that is elevated in 35-40% of CRC patients (Kim *et al*., 2017; Stiksma *et al*., 2014).

Table 1.1. Clinical practice guidelines for CRC

Tumor	Treatment Setting	Aim	Treatment	Regimens
Colon	Adjuvant (after surgery)	Prevent distant metastasis	Chemotherapy	FOLFOX (5-FU, oxaliplatin, folinic acid)
				XELOX (oxaliplatin, capecitabine)
Rectum	Neoadjuvant (before surgery)	Reduce tumor burden and local recurrence	Short-Course Perioperative Radiotherapy	Fractionated Radiotherapy (5x5Gy)
			Long-course Chemoradiotherapy	Radiotherapy (45-50Gy in 25-28 fractions) plus Chemotherapy

1.1.3 Therapy inefficacy

Despite the improvement achieved in anticancer treatments and the development made in targeted cancer therapies, patients do not respond in the same manner, proving that therapies can be efficient and successful for some patients but not for others (Nagle *et al*., 2018) The unique and specific molecular signatures of each tumor are responsible for tumor heterogeneity, which represents one of the reasons why anticancer therapies can be inefficient (Burrel *et al*., 2013). Tumor heterogeneity is characterized by the genetic and phenotypic diversity present in cancer cells subpopulations, leading to distinct behaviours and consequently to different therapy sensitivities. This heterogeneity is observed between tumors in different patients, named intertumoral heterogeneity, which depends on patient-specific factors such as genetic germline and somatic alterations and environmental causes. Moreover, within each individual tumor it is also observed heterogeneity, intratumoral heterogeneity, due to the genetic variability in tumor subclones (Dagogo-Jack and Shaw, 2017). Additionally to cancer cell-intrinsic mechanisms and genomic instability (genetic profile and epigenetic factors), the TME has also a determinant role in tumor response to therapy, modulating its efficacy. The surrounding TME influences tumorigenesis, capable to act in favor or hindering tumor progression, exhibiting tumor-promoting or anti-tumoral profile, respectively. The therapeutic resistance results from the continuous crosstalk between cancer cells and TME that attempts to increase cancer fitness, providing favorable growth conditions (Anari *et al*., 2018). Therefore, the paradox role of TME in tumor progression will have impact in the therapeutic outcome either positively or negatively (Klemm and Joyce, 2015). However, patients are still submitted to treatments according to the "one-size-fits-all" approach, regarding the similarities in tumor type and histological features (Wistuba *et al*., 2011). Consequently, many patients do not benefit from the treatment given, being subjected to unnecessary toxicity and side effects. Thus, the need of personalized medicine, defined as treatment based on tumor genetic and molecular features from an individual patient to improve therapeutic efficacy, is emerging (Stakheyeva *et al*., 2017).

1.2 Cancer avatars for personalized medicine

The singularity of each tumor in an individual patient hinders the development of methods that can predict tumor response. Thus, the capacity to distinguish tumors that will benefit from anticancer treatments (responders), from those who will not (non-responders) remains a challenge. In the 1980s, Patient-derived Xenografts (PDX) were established (Barriuso *et al*., 2015) with an increase in the recent years where many studies have been developing PDX models as a platform for drug screening with applications in preclinical therapeutic evaluation (Williams, 2018). PDXs, also called cancer avatars (Matchett *et al*., 2017), are generated by the implantation of patient primary tumor cells or tissues, derived from surgery, into immunodeficient mice. The tumor samples are first fragmented or digested into cell suspension following its implantation into the murine model. After the establishment of the tumor mass, it is expanded into more recipient mice to increase the number of animals models (Lai *et al*., 2017). This model has been extensively used and explored in cancer research since it provides the

possibility to mimic the original tumors, recapitulating each patient cancer *in vivo.* Beside tumor cells transplantation, PDX also takes in account the TME. Therefore, tumor architecture and heterogeneity may be maintained, leading to a better representation of the tumor biology in the patient (Byrne *et al*., 2017). Thus, it is an ideal model to study tumorigenesis, to comprehend how tumor cells behave and respond to specific drugs and inhibitors (Lai *et al*., 2017). Indeed, this model has been tested to predict therapeutic response in patients, with the aim to provide pre-clinical insights and to guide treatment decisions (Matchett *et al*., 2017). It may dictate the most effective therapy for an individual patient regarding its tumor specific features (clinical, genetic and molecular), allowing also the identification of therapeutic targets (Astone *et al*., 2017). This has been mainly developed in mice and despite the promising achievements made, there are limitations and challenges: the need of immunocompromised mice to avoid PDX rejection; the necessity of a huge amount of sample to generate the xenograft; and highly expensive. But most limiting is time consuming model, where usually the required time for sample engraftment is about 2-4 months, with the possibility to be rejected until at least 6 months; and, among others, the acquisition of mutations due to the tumor expansions made into mice-to-mice may lead to different cells behaviours and responses to treatments (Pompili *et al*., 2016).

1.2.1 Zebrafish avatars in cancer precision medicine

1.2.1.1 *Danio rerio*

Zebrafish (*Danio rerio*) is a small teleost freshwater fish, originally from rice fields and Ganges river of India and Burma. As a vertebrate animal model, zebrafish has been widely used in development biology and vertebrate genetics (Liu and Leach, 2011). It became a very attractive and advantageous model given its characteristics like: high number of offspring (about 200 embryos per zebrafish mating couple, weekly); the small embryos and larvae transparency that allows live-imaging and easy screenings; fast embryo and larvae development (48h to hatch) that occurs *ex vivo*; easy manipulation; fast life cycle (in three months zebrafish reaches the sexual maturity being considered adults); and the low maintenance costs (Taylor and Zon, 2009). Moreover, the zebrafish genome is sequenced, sharing 70% similarities with humans, namely in crucial pathways involved in vertebrate development and cancer that are highly conserved between both species. It is also reported that zebrafish reveal human disease-related genes which turned this vertebrate very popular and extensively used in diseases modeling. Thus, zebrafish arises as a faster and cost-effective *in vivo* model comparing to mammalian ones (Kirchberger *et al*., 2017).

1.2.1.2 Zebrafish xenografts

Due to the advantages described above, the zebrafish arises as a promising *in vivo* model for human cancer studies, with a boost since 2010 (Barriuso *et al*., 2015). The pioneering transgenics for leukemia, rhabdomyosarcoma and melanoma launched zebrafish as a genetic cancer model, where with genetic tools and the development of different transgenic strains is possible to express and study targeted mutations in oncogenes and tumor supressors. This genetic approach is based on the transfer of cancer

mutations from human or mice into zebrafish (trangenesis), or mutating orthologous zebrafish genes (mutagenesis). Recent technologies, such as TALEN and CRISPR/Cas9 tools, also allow zebrafish genome editing.

In addition to the genetic models, zebrafish xenografts have been also a successful approach in oncology precise medicine (Kirchberger *et al*., 2017). Zebrafish xenografts are generated by transplantation of one specie-specific cells into the animal model that can differ in the developmental stage, usually in the perivetilline space, yolk, Duct of Cuvier, brain ventricles or the pericardial cavity. The embryo or larvae transparency allows the direct monitoring of the fluorescently labeled tumor cells offering the possibility to investigate hallmarks of cancer, such as tumor cells proliferation, tumor-associated angiogenesis, invasion and metastasis formation, as well the observation of the tumor and host environment interactions (Taylor and Zon, 2009). The absence of the adaptive immune response until 8 days-post fertilization (dpf) (Tian *et al*., 2017) represents one of the most advantageous feature of zebrafish that allows xenografts engraftment. Thus, zebrafish xenografts are not rejected until that time point, avoiding the need of immunosuppressing agents or radiation, a crucial request for immunocompromised mice (Astone *et al*., 2017).

Several studies have shown that the zebrafish model can also be used as real time *in vivo* drug screening platform, due to its capacity to absorb chemicals through water (Taylor and Zon, 2009). Given its high throughput and fast development, zebrafish can be a very hopeful model to identify therapies that can eradicate tumor cells, and provide clinical insights in less than two weeks (Kirchberger *et al*., 2017). Lee *et al.*, 2005 was the first reported study where a human metastatic melanoma cell line was transplanted into blastula-stage zebrafish embryo (2.25 - 5.25 hours-post fertilization - hpf). The study showed the ability of tumor cells to proliferate and disseminate through the host, maintaining their dedifferentiated phenotype. However, no tumor was formed, suggesting the influence of tumor-suppressing zebrafish microenvironment. The results revealed the ability to use zebrafish as an experimental tool to investigate tumor cells plasticity and tumor-microenvironment communication (Lee *et al*., 2005). Since Lee *et al.*, 2005, many studies were published using distinct cell lines (colorectal, pancreatic and breast cancers, among others) generating zebrafish xenografts. In 2006, Haldi and colleagues injected for the first time a 48hpf zebrafish larvae, using melanoma, colorectal and pancreatic cells lines. This research group optimized several parameters in order to improve the xenografts establishment, and were the first to quantify the injected cells demonstrating that cells could proliferate along time in zebrafish larvae. The results also showed that the different cell lines were not able to migrate in the same rate, suggesting the capacity to represent in zebrafish the heterogeneity of human cells (Haldi *et al*., 2006). In addition, other studies showed the ability of zebrafish to access the metastatic potential of tumor cells (Teng *et al*., 2013).

1.2.1.3 Zebrafish Patient-derived Xenografts

Beside zebrafish transplantation of human cell lines, recently zebrafish Patient-derived Xenografts (zPDX) arose as an alternative cancer model. zPDX can represent an opportunity to get a

personalized approach for cancer treatment, where patient prognosis and evaluation of drug responses can be assessed in real time, with a main goal: identification of the most appropriate therapy for a patient-specific cancer (Astone *et al*., 2017).

The pioneering study Marques *et al*., (2009) showed for the first time the possibility to transplant primary human tumors in zebrafish. Pancreas, colon and stomach primary tumors were transplanted either as tissue fragments or primary human cell suspension into embryo and larvae yolk. Both tissue fragments and human cell suspension had metastatic behaviors, disseminating through the zebrafish organism (1-3 days-post transplantation/injection). Invasiveness capacity was also assessed comparing non-tumoral and tumoral pancreatic cells, where only the last ones were able to form metastasis. Therefore, it is also possible to investigate patients' primary tumors behaviors using the zebrafish model, since it allows the study of the intrinsic properties of cancer cells (Marques *et al*., 2009).

Several studies have been developed aiming the correlation between zPDX behavior and response to therapies, in order to obtain clinical insights and guide treatment decisions: Welker and colleagues (2015) using glioblastoma patient-derived cell lines for the standardization of zPDX model, submitting the human xenotransplants to glioblastoma treatments; Bentley *et al*., (2015), using zebrafish model as pre-clinical therapeutic platform for leukemia patients; and also two recent studies regarding breast (Mercatali *et al*., 2016) and gastric cancer (Wu *et al*., 2017b) suggesting that zPDX can reflect clinical patient prognosis and might be a promising preclinical approach for personalized medicine.

Although the progress achieved with zPDX for precise cancer medicine, there is still a lack of studies correlating patient response and zPDX response to the same treatment (Astone *et al*., 2017). Before this approach start to be used in clinical assays, it is essential to test zebrafish *in vivo* model predictability. Following this purpose, in 2017, Fior and colleagues tested the capacity to use zebrafish xenotransplants as a platform for drug screening. Firstly, in order to unravel the ability of this *in vivo* model to reveal intertumoral and intratumoral heterogeneity, human colorectal cancer cell lines isolated from different patients' as well isogenic pairs (SW480/SW620 and HCT116/Hke3, respectively) were injected in the 48hpf larvae. The results showed that in 4 days the hallmarks of cancer, such as proliferation, metastatic and angiogenic potentials were recapitulated, and that it was possible to detect distinct behaviors *in vivo* with high single-cell resolution. It was also tested the different CRC cell lines sensitivities to ChT, where even isogenic CRC cell lines with similar genome profiles exhibited distinct responses to therapies. CRC zPDX from surgery human samples were also generated, submitting the zPDX to the same ChT regimen as their matching patients (Adjuvant ChT). The promising results showed that zPDX maintained their original features; in four out of five zPDX it was possible to anticipate if the tumor would relapse or not after treatment. This recent study suggests that the zebrafish model can be used as a tool to predict tumor patient-specific response to the recommended ChT (Fior *et al*., 2017).

1.3 Radiation

X-rays discovery by Wilhelm Conrad Rontgen, in 1895, and radium studies by Marie Curie prompted the application of radiation in the clinic. Radiation is widely used for cancer treatment due to

its capacity to induce tumor cellular damage while minimizing the surrounding tissues toxicity (Baskar *et al*., 2012). About 50% of cancer patients are submitted to Radiotherapy (RT), where it can be given with the intent of cure or as a palliative treatment (Weichselbaum *et al*., 2017).

1.3.1 Radiation and biological effects

Ionizing radiation (IR) produce ions from electrons ejection, and it can be divided in electromagnetic radiation (X-rays and γ-rays) and particulate radiation which includes neutrons and charged particles (α and β particles) (Elgazzar, 2006). X-rays and γ-rays are the common radiation type used in cancer therapy, generated by electrons excitation and decay of radioactive substances (radium, cesium, cobalt-60, etc.), respectively (Weichselbaum *et al*., 2017). Both radiations are considered low linear energy transfer (LET) due to the small quantity of deposited energy (Baskar *et al*., 2014).

DNA is the main biological target of radiation. The cellular damage can be the result of IR direct action on the genetic material (causing DNA double-strand breaks (DSB), single-strand breaks (SSB), DNA crosslinks and DNA-protein crosslinks), or indirectly, from the production of free radicals (reactive oxygen species (ROS) and reactive nitrogen species (RNS)) due to radiation or excitation of the cellular water component (radiolysis). From all, DNA DSBs represent the most lethal type of DNA damage induced by radiation (Wang *et al*., 2018). In response to DNA damage, three kinases, named Ataxia Telangiectasia mutated (ATM), AT-related (ATR) and DNA-dependent protein kinase (DNA-PK) are activated. ATM is the major kinase involved in DNA damage response to DSB promoted by IR, inducing cell cycle arrest in order to repair the injury. Cell cycle arrest allows the recruitment of DNA repair machinery, where DSB are recovered mainly by two pathways: Homologous recombination (HR), that requires the sister chromatid as a template to synthesize a new DNA strand, occurring preferably during S/G_2 phases; or non-homologous end joining (NHEJ) that joins rapidly the two broken DNA ends, mainly in G_1, without resection (generation of single-stranded DNA (Maier *et al*., 2016). Phosphorylated ATM (activated) acts directly in CHK1 and CHK2 transducers (checkpoint kinases-1and -2), which in turn activate the tumor suppressor p53, which will accumulate in the nucleus and act as a transcriptional factor. Then, p53 activates p21 (cyclin-dependent kinase inhibitor), resulting in G_1 cell cycle arrest and G_2/M transition phase blockade, by inhibition of CDK4/6 and CDK1, respectively. During the damage signalling, ATM also phosphorylates rapidly the histone H2AX (γH2AX) at serine 139 and tyrosine 142 near to C-terminal end, amplifying the damage signals and serving as a scaffold for DSB repair machinery assembly. However, if the damage is not repaired it will lead to cell death (Goldstein and Kastan, 2015; Maier *et al*., 2016).

The therapeutic effect of IR is achieved when the sustaining proliferative capacity of tumor cells is inhibited either by affecting cell cycle or impairment of DNA repair. Cancer cells are characterized to be more sensitive to DNA injury comparing to the non-tumoral cells, given its inefficient and slower DNA repair machinery (Baskar *et al*., 2014). Thus, irradiated cancer cells, with low ability to repair DNA damage, accumulate DBS, while healthy cells are able to repair their genetic material in a faster and efficiently rate. The genomic instability caused by RT can lead to different types of cell death, such as (Maier *et al*., 2016):

1) *Apoptosis* (programmed cell death), the major type of cell death observed after RT, characterized by cell shrinkage, DNA fragmentation and apoptotic bodies formation. p53 nuclear accumulation activates the pro-apoptotic Bax and Bak proteins, triggering mitochondria and consequent permeabilization with cytochrome *c* release. Therefore, the apoptosome complex is formed and activated Caspase9 subsequently activates Caspases3, 6 and 7 (apoptosis effectors), leading to cell death (Maier *et al*., 2016);

2) *Mitotic catastrophe*, consequence of cell cycle failure, before or during mitosis, which is responsible for aberrant chromosomes segregation resulting in abnormal nuclei morphology and giant cells (Castedo *et al*., 2004). Additionally to apoptosis, mitotic catastrophe it is also very frequent in irradiated cells (Baskar *et al*., 2014);

3) *Necrosis* (non-programmed cell death), defined by the disruption of cell membrane with loss of the intracellular components (Baskar *et al*., 2014);

4) *Senescence*, cellular stress response resulting in cell growth arrest but still metabolically viable, where cells become enlarged and flattened (Collado and Serrano, 2006). It can result from prolonged p53 activation and subsequent expression of p21, responsible for permanent G_1 phase arrest (Maier *et al*., 2016);

5) *Autophagy*, where the intracellular components are degraded and digested, with double-membranes vacuoles formation and autophagosomes accumulation (Todd *et al*., 2009).

Additionally to the injury made in the cellular nucleus (chromatin aberrations), which appears to be more radiosensitive than the cytoplasm components, radiation is also capable to affect the cellular membrane, therefore interfering with cell signalling, immunogenicity and the surrounding microenvironment (Wang *et al*., 2018).

1.3.2 Fraction and dose

Despite the action of radiation in cancer cells, the biological effectiveness depends on many factors, such as the total LET dose given, the RT regimens, the radiosensitivity of each tumor and time to induce the biological effects (Baskar *et al*., 2014, Gasinska *et al*., 2004).

1.3.2.1 Conventional Vs Hypofractionated Radiotherapy

Since x-rays discovery, radiation was been delivered in low dose fractions for cancer treatment (1.8-2 Gray (Gy)/fraction) for several weeks, named conventional fractionated RT (Grays are the measure of IR that represents the energy absorbed from 1 joule of energy by 1 kilogram of material, (Barcellos-Hoff *et al*., 2005)). The fractionated scheme relies on its capacity to spare the surrounding tissue while maximizes the radiation dose applied to the tumor location (Brown *et al*., 2008). However, conventional RT therapeutic efficacy decreased in tumors with greater ability to repair the damage between fractions. To overcome this challenge, larger IR doses per fraction started to be delivered in shorter time periods, denominated hypofractionated radiation (Folkert and Timmerman, 2017). In 1951, neurosurgeon Leksell attempted for the first time the delivery of high RT doses in non-malignant brain lesions (Lesksell, 1951) and since then, hypofractionated RT was mainly applied in intracranial lesions

and in cancer palliative treatment, due to the assumption that this regimen could affect the tumor surrounding healthy tissues (Hellevik and Martinez-Zubiaurre, 2014).

Thanks to the improvement in technology is now possible to deliver high IR doses to a defined targets with accuracy, either in single dose or in few fractions. Stereotactic Body Radiation Therapy (SBRT) also known as Stereotactic Ablative RT (SABR) is an increasingly accepted RT technique based on hypofractionated radiation, where larger doses per fraction are delivered in shorter time periods (Folkert and Timmerman, 2017). SBRT biological effectiveness has been proven for several types of cancer namely Non-Small-Cell Lung Cancer (NSCLC) (Nyman *et al*., 2016), prostate cancer (Stokes *et al*., 2017) and for CRC (5x5Gy fractionated regimen) (Cutsem *et al*., 2016).

1.3.2.2 Hypofractionated Radiotherapy: Fractionated Vs Single-High Dose

Clinical RT schemes are based in dose fractionation that consists in diving the therapeutic dose in smaller doses per fraction delivered for a certain period of time. The clinical importance of fractionated RT (FRT) is described by the five radiobiological "Rs" (Wedenberg, 2013; Klement, 2017):

1) Repair: dose fractionation allows normal healthy tissues repair, whereas cancer cells are more likely to remain damaged due to the low repair capacity;
2) Redistribution: Cell cycle G_2/M phase appear to be more radiosensitive than S phase, which is more resistant to radiation. Fractionation promotes cell redistribution to the sensitive phase that turn cells more vulnerable to radiation damage;
3) Reoxygenation: a hypoxic TME can lead to cells radioresistance. Thus, fractionated RT allows reoxygenation between fractions enhancing radiation effects;
4) Repopulation: Prolonged treatment enables both non-tumoral and tumoral cells proliferation, which for the last ones can result in tumor regrowth;
5) Radiosensitivity: fractionated biological effects also depend on the intrinsic radiosensitivity of each cell.

Despite the uncontested effectiveness of FRT radiobiology (Brown *et al*., 2008), Single-High Doses RT (SHD-RT) showed to be useful in the clinic mainly due its benefits in a palliative context, namely for bone metastasis and metastatic spinal canal compression (De Felice *et al*., 2017; Hoskin *et al*., 2017, respectively), with evidences of its application for NSCLC (Hof *et al*., 2003). Moreover, Brown *et al*., 2008 mentioned that SHD-RT can elicit a high tumor control, suggesting that this regimen might elicit different biologic effects. In 2006, Horsman and colleagues evaluated SHD-RT (1x20Gy) and FRT (2x10Gy) impact in tumor growth, where both regimens induced tumor responses, however Single-High Doses suggested to be more effective as a treatment than FRT (Horsman *et al*., 2006). Moreover, the increasingly interest in the hypofractionated regimen led to another study were it was studied the biological impact of FRT (5x10Gy) and SHD-RT (1x50Gy) on plant growth development (Guedea *et al*., 2013). The study showed the effective impact of SHD-RT in slowing plant cell growth, where small height phenotype predominated in plants submitted to SHD-RT comparing to FRT treated plants. Despite the obtained results in plant cells, Guedea and colleagues suggested more studies to

assess SHD-RT in human cancer tissues. It has been also suggested the SHD-RT impact in the endothelial vasculature, inducing vascular damage and consequent tumor clearance (Brown and Koong, 2008; Folkert and Timmerman, 2017), being also studied the impact of both RT regimen in TME and how they can modulate differently the immune system (Deloch *et al*., 2016). In general, SHD-RT arise as a convenient approach that may represent time and cost-effective advantages. However, it requires more investigation and validation for clinical purposes.

1.3.3 Zebrafish xenografts irradiation

Radiation has an important role in zebrafish immune system ablation and it is mainly used to prevent transplanted cells (xenografts) rejection, in adult zebrafish studies. Sublethal Single-High Doses of 20-25Gy are delivered to immunosuppress the *in vivo* model, and at least more than 80% of zebrafish tolerate this range of IR (Taylor and Zon, 2009). In addition to radiation immune suppressive effect, radiation was delivered to embryos xenografts with the aim the development of new methods that allow the improvement of radiation effect (e.g. Lally *et al*., 2007; Geiger *et al*., 2008). However, no studies have been reported where radiation effect is tested in zebrafish xenografts response, or either aiming the development of RT screening platform using zebrafish for a personalized medicine.

1.3.4 Radiation and macrophages

Macrophages are one of the major cellular component present in human tumor microenvironment, with variations from 10% to 65% among the different tumors, usually present in tumor margins and near to necrotic areas (Genard *et al*., 2017). These immune cells are responsible for orchestrating several interactions in the TME, important in cancer development with a pivotal role in therapeutic response (Pinto *et al*., 2016). Macrophages phenotype heterogeneity is responsible for its dual character in antitumor immunity: M1-like macrophages are considered the immune stimulatory cells that produce pro-inflammatory mediators', involved in bacterial clearance and tumor cytotoxicity; M2-like macrophages, on the other hand, are involved in immune suppression with an anti-inflammatory profile. Therefore, M1-like are considered tumor suppressors macrophages and M2-like, the tumor promoters'. Radiation effect in macrophages is also determinant for RT outcome given its capacity to modulate their phenotype polarization, where several studies have suggested that macrophages reprograming is radiation dose-dependent (Genard *et al*., 2017).

1.3.5 Radiotherapy biological effect in zebrafish larvae xenografts

Previous work from the Lab (Póvoa and Fior, unpublished) tested for the first time SHD-RT (1x25Gy) biological impact in zebrafish larvae xenografts, using the colorectal carcinoma cell lines: HCT116 *KRAS*^{G13D} isolated from a primary tumor, reported as radiosensitive; and Hke3 generated from HCT116 by homologous recombination (HR), reverting the oncogene phenotype, that suggested to be radioresistant. For a less time-consuming assay and for logical reasons, SHD-RT regimen (1x25Gy delivered in a single RT session) was used, based on the total dose of the FRT (5x5Gy) given in the clinical setting. In addition, SHD-RT combination with 5-FU ChT (CRT) was also tested. The results

showed a stronger RT anti-tumor effect for HCT116, with significant tumor size downsizing, decreased proliferation capacity and increased apoptotic cell death, comparing to Hke3 where no significant differences were observed between the irradiated xenografts and the non-irradiated controls (Figure 1.1I-K). Also, CRT exhibited a synergistic effect in HCT116 cells, whereas Hke3 did not respond significantly to the treatment combination. These preliminary results showed the ability of the zebrafish model to assess distinct tumor responses to RT, regarding cancer cells radiosensitivity. The results suggested that SHD-RT (1x25Gy) might allow to discriminate xenografts that respond to RT from those who not (non-responders). These promising results suggest the possibility of testing zPDX as a potential therapy-screening platform for RT clinical insights.

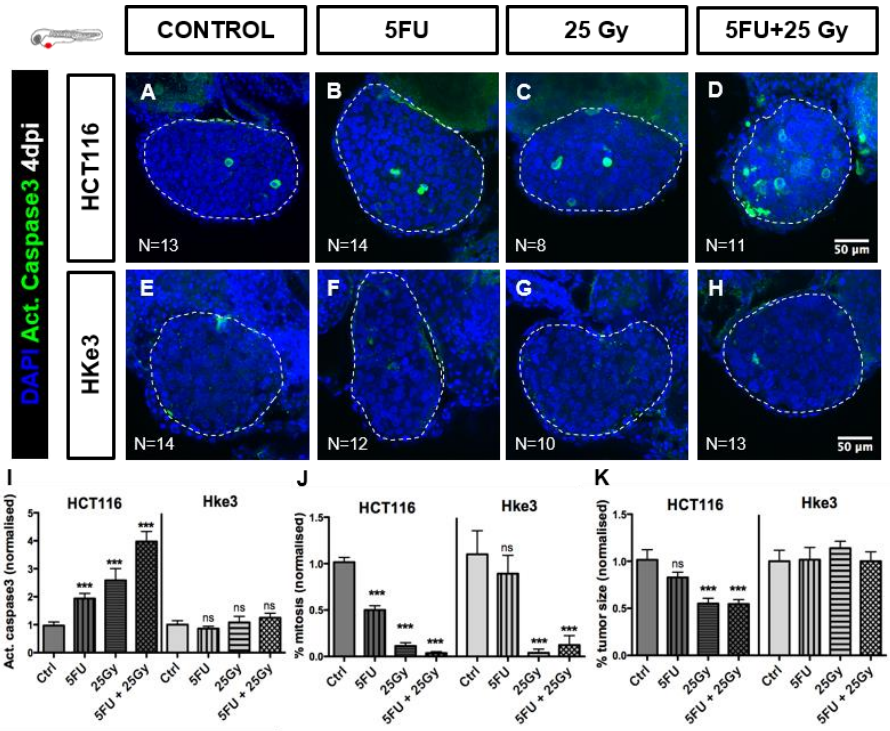

Figure 1.1. SHD-RT (1x25Gy) can determine CRC xenografts radiosensitivity/radioresistance. Human CRC cell lines (HCT116 and Hke3) were injected into the PVS of 2dpf zebrafish and submitted to 5-FU ChT for three consecutive days (B and F), SHD-RT (1x25Gy) (C and G) and 5-FU and 25Gy combination (D and H). At 4dpi, zebrafish larvae were euthanized and fixed. Apoptosis (activated Caspase3) (I), mitotic figures (DAPI) (J) and tumor size (DAPI cells number) (K) were analyzed and quantified for the three treatment conditions and compared with non-treated controls. I-K are the normalized results to the respective controls, and are average from two independent experiments where the total xenografts number analyzed is indicated in the images. The results (I-K) are expressed as AVG±SEM. The dashed white line present in A-H images represents the individual tumor area (ROI). All pictures (A-H) are at the same magnification (40x). Scale bar (50µm). Statistical analysis was performed using the unpaired non-parametric Gaussian distribution and Mann-Whitney test. *P value*, ***P<0.001; ns, nonsignificant.

1.4 Aim

Recently, Fior and colleagues developed zPDX for personalized medicine to quickly screen the recommended ChT for CRC with very promising results in the Adjuvant setting. However, for zebrafish xenografts to be used in the clinic, it is essential to test its predictive value with more patients, in different types of cancers but also importantly in a more controlled clinical setting as the Neoadjuvant (NA) setting. Rectum NA setting (SCPRT, 5x5Gy, or its combination with Chemotherapy (CRT)) provides the ideal conditions to test zPDX predictability due to the opportunity to obtain CRC biopsies as well tumor response can be assessed in a short controlled time period (2-4 months), following treatment.

Laboratory preliminary work tested the NA setting in CRC and demonstrated that is possible to distinguish radiosensitive/radioresistant zebrafish xenografts. However, for convenient practical reasons the radiation regimen used (SHD-RT, 1x25Gy) was different from the one given in the clinic for CRC patients, FRT (5x5Gy), raising the question whether the single dose (1x25Gy) was good enough as a proxy to distinguish radiosensitive tumors (responders) from radioresistant (non-responders).

Therefore, the main goal of this thesis was to compare both RT protocols and test if SHD-RT protocol is suitable for determining radiosensitivity and radioresistance.

The ultimate goal of the laboratory is to test zPDX ability to screen CRC patients for RT and test the predictability of the assay. For that, the correlation between patient tumor response in the clinic with their matching zPDX to the same treatment needs to be evaluated (Figure 1.2). The development of this protocol is essential to develop this assay further, contributing hopefully, in the future, for personalised therapy, sparing patients from unnecessary treatments (when they are resistant).

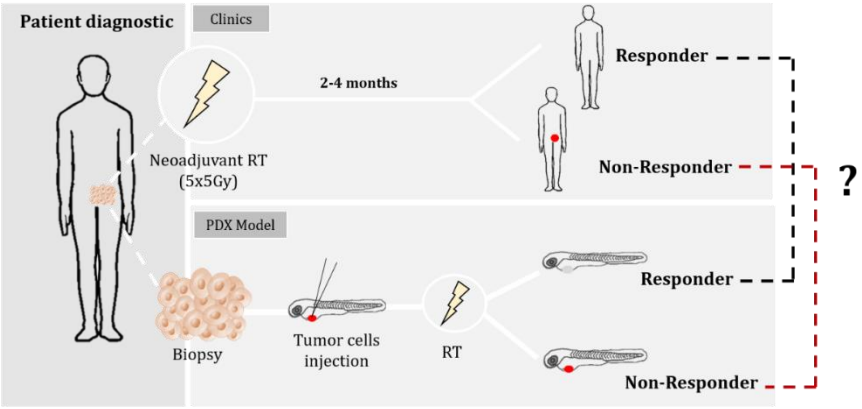

Figure 1.2. Zebrafish model evaluation as a potential Radiotherapy screening platform. Schematic representation of our Lab main goal: test zebrafish capacity to predict tumor response to Radiotherapy (RT). Zebrafish Patient-derived Xenografts (zPDX) are generated by injection of biopsies cells suspension into a 2dpf zebrafish larvae. Following injection day, zPDX are submitted to Neoadjuvant Radiotherapy, the same treatment as their matching patient. In one week, zPDX tumor response can be assessed and compared with the matching patient response in the clinic (2-4 months). If zebrafish predictability is showed, it is expected that patient tumor response correlates with the matching zPDX response: patients responders to Neoadjuvant Radiotherapy would correspond to the radiosensitive zPDX, whereas the non-responders patients would match with the radioresistant zPDX.

2. Materials and Methods

2.1 Cell culture

Colon cancer cell line, HCT116, donated by Dr.Ângela Relógio (Institute for Theoretical Biology, Berlin), was tested for mycoplasm and authenticated through Short Tandem Repeat (STR) profiling (karyotyping isoenzyme analysis). Before experiments, HCT116 cells were expanded and maintained in filtered Dulbecco's Modified Eagle Medium (DMEM) (Sigma) supplemented with 10% Fetal Bovine Serum (FBS) (Sigma) and 1% Penicillin−Streptomycin (HyClone) in a humidified atmosphere containing 5% CO_2 at 37°C (inCu Safe).

2.1.1 Cells thawing and freezing

To preserve their viability, cells were frozen in cryovials (Nunc) containing freezing medium (90% FBS plus 10% Dimethyl Sulfoxide (DMSO)) in liquid nitrogen. Before their usage they were thawed quickly in a water bath at 37ºC. In the laminar flow, cryovials content were carefully transferred to a 15mL falcon with 10mL of DMEM. After centrifugation (1200 rotations per minute (rpm) during 4 minutes), the supernatant was removed, eliminating the DMSO present in the freezing medium, and the pellet was resuspended in 2mL of DMEM. The homogenised pellet was gently transferred to individualized T75cm^2-flasks (Corning) and cultured as described above. Right after 2-3 passages, cells were expanded to maintain the cell lines batch and to avoid the gain of *in vitro* cell mutations. To freeze the cells it was added freezing medium, previously prepared. Afterwards the pellet homogeneized in FBS and DMSO (used to prevent ice crystals formation) was distributed into 2mL cryovials, which were placed in a freezing container at -80ºC overnight and transferred to the liquid nitrogen, at -196ºC in the next day for long-term preservation.

2.1.2 Cells expansion

The cells kept in culture were submitted to passages (no more than fifteen), performed twice a week once they achieved 70%-80% of confluence. Firstly, the culture medium was removed, cells were washed with 1x Dulbecco's phosphate-buffered saline (DPBS) (Gibco, Life Technologies) and detached with TryplE for 2-3 minutes at 37ºC. In order to obtain the pretended cell dilution, the volume of trypsinized cells was transferred to a new T75cm^2-flask (e.g. if the required dilution was 1:3, a third of the total volume of trypsinized cells was placed into the T75-flask). At last, fresh culture medium was added to the flask (usually 9-10mL of DMEM) and placed at 37ºC.

2.1.3 Cells staining

Cells were grown until 70% confluence, washed with 1x DPBS and stained in the flask with a red fluorescent dye, DiI, (Vybrant CM-DiI; Molecular Probes, Life Technologies, 4µL/mL in 1x DPBS) or DeepRed dye (CellTracker, Molecular Probes, Life Technologies, 1µL/mL in 1x DPBS) for 10 minutes at 37°C followed by 15 minutes on ice in darkness (Table 2.1). After dye removal, cells were washed with 1x DPBS, detached with 2mL of DPBS-EDTA (2mM EDTA, Sigma) for 5 minutes at 37ºC

followed by scraping from the flask. The detached cells were distributed into two 1.5mL eppendorf tube that were centrifuged for 4 minutes at 1200rpm. The two pellets were resuspended in 60µL of DMEM and placed together in only one eppendorf tube. The cell viability was assessed by the trypan blue exclusion method, and cell number was determined by hemocytometer counting (Neubauer) (Blau Brand) (described in detail in section 2.1.4). Finally, cells were centrifuged (1200rpm for 4 minutes) and resuspended in 1x DPBS to a final concentration of 0.25×10^6 cells/µL. The cells were kept on ice throughout the zebrafish injection.

Table 2.1. Specifications of the used fluorescent dyes, and the respective dilution in 1x DPBS.

Dye	Colour (Abs, Em)	Supplier	Dilution factor in 1x DPBS
CM-DiI	Red (549nm,565nm)	Vybrant,Molecular Probes, Life Technologies	1:200
Deep red	Infra-Red (Cy5) (630nm,660nm)	CellTracker, Molecular Probes, Life Technologies	1:1000

2.1.4 Cell counting

For cell counting, 10µL of the total volume of the pellets resuspended in DMEM, described in the previous section, were diluted in trypan blue, performing a 1:100 cell dilution. From this dilution, 10µL was pipetted and placed in the hemocytometer. Since the trypan blue is only permeable to disrupted cell membrane, the viable cells were translucent, while dead cells were stained in blue. The viable cells were counted in the four hemocytometer quadrants (each quadrant corresponding to $0.1mm^3$), and cell concentration was calculated according to Equation 1. Therefore, the total number of cells was assessed by Equation 2, according to the total volume of the pellet resuspended in DMEM. Finally, Equation 3 was done to determine the volume of 1x DPBS to resuspend the pellet in order to obtain a final concentration of 0.25×10^6 cells/µL. The percentage of cell death was also estimated using the Equation 4.

Equation 1. $$\text{Cell concentration (cell/mL)} = \frac{\text{Viable cells number}}{\text{4 quadrants}} \times 10^2 (\text{dilution factor}) \times 10^4\ \text{mm}^3\text{mL}^{-1}$$

Equation 2. $$\text{Total cell number (millions)} = \text{pellet volume (mL)} \times \text{cell concentration (cell/mL)}$$

Equation 3. $$\text{Final volume (µL)} = \frac{\text{Total cell number}}{0.25\times10^6}$$

Equation 4. $$\text{Cell death (\%)} = \frac{\text{Dead cells number}}{\text{Total cells counted (viable and dead)}} \times 100$$

2.2 Colorectal cancer patient samples processing and staining

The CRC patient samples were kindly provided by the Surgery and Histopathology Units of Champalimaud Clinical Centre and Hospital Professor Doutor Fernando Fonseca (Amadora Sintra). All samples used were obtained with written informed consent and the study was approved by the Ethics Committees of both Hospitals.

After samples arrival in collection medium (described in detail in Appendix, Table 5.4), they were successively washed in 1x DPBS. The washed sample was cut into small fragments of tissue and centrifuged at 1200rpm for 4 minutes, in a 50mL falcon with 1x DPBS to remove possible contaminations. A 40µm strainer (Fisher Scientific) was used to discard the 1x DPBS used in the centrifugation, and the sample fragments were transferred to a 2mL cryovial with freezing medium (90% FBS and 10% DMSO), and frozen at -80ºC. In the following day the cryovials were placed at -196ºC in liquid nitrogen.

On the injection day, the selected samples were thawed at 37ºC water bath for 2 minutes, approximately. The cryovial content was passed through a 40µm strainer, discarding the freezing medium and saving the sample fragments. All the mix solutions used are described in detail in Table 5.4 (Appendix). Three-time series of wash with 1x DPBS were done and the sample was further rinsed in Mix1, with the aim to disrupt the big cells clusters connection and to obtain a cell suspension. The mechanically fragmented tissue was centrifuged in Mix1 at 1000rpm for 4 minutes at 4ºC in a 50mL falcon. The supernatant was removed, and the pellet obtained was resuspended in 1mL of Mix1, following its passage now in a 70µm strainer. The remaining fragments on the top of the strainer were collected to a 2mL eppendorf with Mix2 for digestion and labelling with DiI dye, 8 minutes at 37ºC (water bath). The digested sample was then passed through a new 70µm strainer, mixing the labeled cells with the non-labeled. The total amount of cell suspension was transferred to a 15mL tube and centrifuged in Mix1 900rpm for 4 minutes at 4ºC. The pellet was resuspended with 1mL of Mix3 and a last centrifugation was performed in the same conditions. Finally, the supernatant was carefully removed, remaining approximately 20µL of Mix3 with the pellet to have the proper density of cells to inject in zebrafish larvae.

2.3 Zebrafish care and handling

All *in vivo* experiments were performed using zebrafish (*Danio rerio*), which was handled according to European animal welfare regulations and standard protocols. For the experiments were used different genetically modified zebrafish lines described in Table 2.2. With exception of the macrophages experiments that were performed in the Mpeg and Mpeg:TNFα transgenics, zebrafish transgenic lines were randomly selected. All zebrafish were maintained in the Champalimaud Foundation Fish Facility.

The adult zebrafish were maintained in 3.5L tanks with running water, at 28ºC, having a 14/10 photoperiod (light/dark). Each tank contained both male and female fish, with a maximum population of 30 fish per tank and were fed twice a day by the Fish Facility team.

Table 2.2. Summary of the used zebrafish transgenics and the respective description.

Zebrafish transgenic	Genetic construction	Description	Uses
Fli	Fli1:EGFP	FLI1 is an erythroblast transformation-specific transcription factor, required for angiogenesis	Labels endothelial cells and lymphatic vessels in green (Lawson and Weinstein, 2002)
Mpx	Mpx:GFP	GFP is expressed under the neutrophil-specific myeloperoxidase promoter (mpx)	Labels neutrophils in green (Renshaw *et al*., 2006)
Pu.1	Pu.1:Gal4 UAS:GFP	GFP is expressed under Pu.1 control, an early macrophage marker. Pu.1 regulates specification and maturation of macrophages and neutrophils in a dosage-dependent manner	Labels myeloid lineage in green (Peri and Nüsslein-Volhard, 2008)
Casper	w2 (nacre), a9 (roy) double mutant	Lacks melanophores (w2) and iridophores (a9)	Complete lack of all melanocytes and iridophores in both embryogenesis and adulthood (White *et al*., 2008)
Nacre	w2/w2 mutant	Complete lack of melanophores (w2) due to the mutation of *mitfa* gene involved in the development of melanophores	Melanophores lack throughout development, however have iridophores (White *et al*., 2008)
Mpeg	mpeg1:mCherry	mpeg1 promoter drive the expression of zebrafish embryonic macrophages	Labels macrophages in red (Ellett *et al*., 2010)
Mpeg:TNFα	mpeg1:mCherryF/ tnfα:eGFP-F	TNFα, a central inflammatory cytokine and a marker of M1-like macrophages, is used to discriminate macrophage subsets during intravital imaging	Labels macrophages in red which turn green in the presence of inflammatory macrophages (M1-like) (Bernut *et al*., 2016)

2.3.1 Adult zebrafish crosses, housing and embryo harvesting

The present study required the usage of zebrafish larvae with 2 days post-fertilization (2dpf). To obtain them, adult zebrafish were crossed three days in advanced. The crosses, with male and female fishes (1:3 proportion), were performed in slopping breeding tanks to create the ideal breeding conditions. The slope allows the eggs to fall, preventing them to be eaten by the adult fish and it also mimics the shallow waters where zebrafish mate in their natural habitats. To each breeding tank it was added synthetic algae to improve environment enrichment. On the morning after the crossing, the embryos were harvested and placed into Petri dishes with embryo medium (E3, more details in Appendix Table 5.1) (~50 embryos per Petri dish), while the adult zebrafish were transferred to the original tanks. In the end, all Petri dishes were incubated at 28ºC until 2dpf.

2.4 Tumor cells microinjection in zebrafish larvae

On the injection day, the Petri dishes with 2dpf zebrafish larvae were cleaned by removing all dead embryos. The hatched larvae (already out of the chorion) were separated from the embryos (larvae inside the chorion), and transferred to a new Petri dish with E3 medium. For dechorionation, pronase

was added to the E3 medium (see Appendix Table 5.2) and Petri dishes were placed in the incubator at 28ºC. Few hours later, E3 medium was replaced and larvae were ready for cell microinjection.

Previously to zebrafish injection process, larvae were anesthetized with 1x Tricaine (diluted from 25x Tricaine in E3 medium, described in Table 5.3 in Appendix). Agar plates (3% in destilated water, VWR chemicals Prolabo) with stripes were prepared to keep the zebrafish larvae aligned. For the injection of fluorescently labeled HCT116 cells (xenografts) or the cell suspension from patient samples (zebrafish Patient-derived Xenografts, zPDX), needles made from glass capillaries (World Precision Instruments, Borosilicate Glass Capillaries, 1mm thickness) were prepared using a Laser-Based Micropipette Puller (Sutter Instrument P-2000). The loaded needle was attached to the tip of a pneumatic injector (World Precision Instruments, Pneumatic Pico pump PV820), which was used for the injection of the tumor cells into the perivitelline space (PVS) of 2dpf zebrafish larvae, assisted by a fluorescence scope (Zeiss Axio Zoom.V16). The injected larvae were carefully placed into a Petri dish with 1x Tricaine for approximately 30 minutes, in order to keep both the larvae and the tumor stable during the recovery phase and wound healing process that follows injection. After that, 1x Tricaine medium was replaced by E3 medium and larvae were placed at 34ºC (compromised temperature between optimum zebrafish development temperature (28ºC) and optimum human cells temperature (37ºC)). In the following day (1dpi), zebrafish were screened: for the HCT116 xenografts, xenografts were classified according to the tumor size (Figure 2.1): ++ (tumor smaller than the size of the larvae eye); +++ (tumor with the same size of the larvae eye); ++++ (tumor bigger than the larvae eye); for the zPDX, the screening was performed according to the presence or absence of a stained tumoral mass. The non-successful injected larvae were discarded and euthanized.

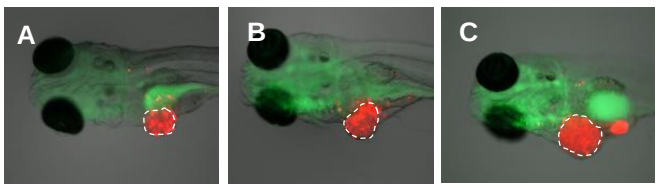

Figure 2.1. Xenografts (HCT116) screening according to tumor size. At 1dpi, CRC xenografts were classified regarding their tumor size: A) ++ xenograft smaller than the size of zebrafish eye; B) +++ xenografts with the same size of zebrafish eye; and C) ++++ xenografts bigger than the size of zebrafish eye.

2.5 CRC xenografts irradiation

One day post zebrafish injection (1dpi), the xenografts (HCT116) previously scored were randomly distributed in three experimental conditions: Control (non-treated larvae), FRT protocol (5x5Gy irradiation) and SHD-RT protocol (1x25Gy irradiation). For the different conditions, 6 well plates were used in which the xenografts were kept throughout the experiment (no more than 12 larvae per well), renewing the E3 medium daily. In the same day, xenografts started the Radiotherapy (RT) regimen: 10 minutes before the treatment, E3 medium was replaced by 1x Tricaine to anesthetize the zebrafish larvae and to guarantee their immobilization on the bottom of the well during the RT session. The irradiation sessions were handled by the Radiotherapy Unit Team of Champalimaud Foundation. Figure 2.2 represents the radiation scheme delivered, where the injected larvae submitted to the FRT

protocol received 5Gy daily fractions for five consecutive days, totalizing 25Gy dose, while the xenografts subjected to SHD-RT (1x25Gy) were irradiated in only single radiation session. The X-rays beam, a LET ionizing radiation, (5Gy and 25Gy) was delivered via linear accelerator (Truebeam, VARIAN Medical System). Immediately after the irradiation, 1x Tricaine was replaced by new E3 medium and larvae were placed at 34ºC until the end of the experiment. In the end of the assay, the xenografts were fixed in FA 4% (4ºC overnight) and transferred to MeOH 100% (-20ºC) on the following day.

Prior to all RT experiments, the irradiation procedure was adapted for zebrafish larvae. Initially, a 6 well plate computed tomography scan was taken, with the same volume used in the radiation experiments (6mL of E3 per well), to further calculations, performed by the Radiotherapy Unit Team: to deliver a 5Gy or 25Gy irradiation, a laser, with the plate center as the reference point, was emitted (100cm at the plate surface) with 6MV energy laser, in 30x30cm area. Thus, the entire 6 well plate received the same desired irradiation X-rays dose.

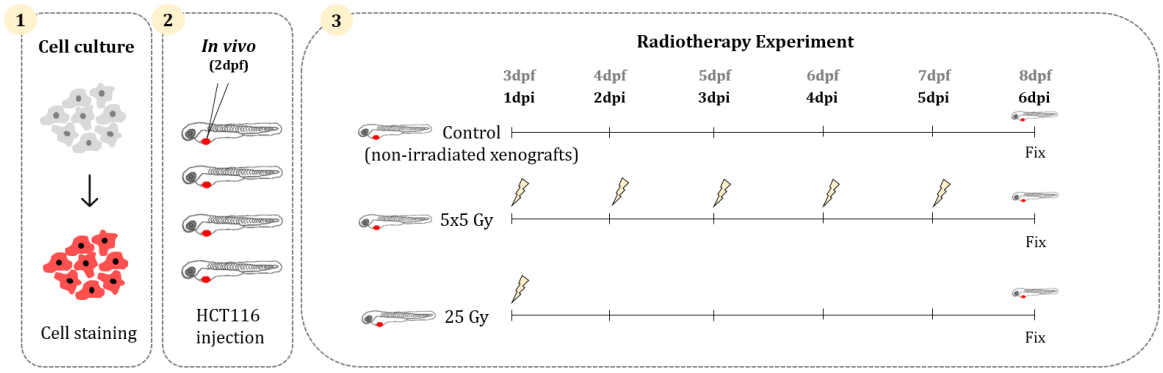

Figure 2.2. Schematic representation of xenografts experimental set up. Primarily, CRC HCT116 cells were stained (1), and injected into the PVS of a 2dpf zebrafish larvae, generating xenografts (2), following radiation treatment (3). The experimental set up illustrated in 3 represents the scheme performed for both RT protocols (SHD-RT, 1x25Gy and FRT, 5x5Gy), until 6dpi. At 6dpi, all the xenografts were fixed and processed for immunofluorescence assay.

2.6 Zebrafish Patient-derived Xenografts drugs administration and irradiation

The following process was performed for several zPDX that were generated during the Masters year in Champalimaud Foundation, mainly by Bruna Costa – a Post-Doc colleague, were I was involved to help.

The 1dpi colon and rectum zPDX were randomly distributed in different treatment conditions according to the recommend therapy for each cancer type (Figure 2.3): Colon zPDX were usually submitted to FOLFOX (5-FU+Oxaliplatin+Folinic Acid in E3 medium) or 5-FU (in E3 medium) Chemotherapy (ChT), for 4 consecutive days, replaced daily; rectum zPDX were subjected to SHD-RT (1x25Gy) in petri dishes (no more than 20 larvae per dish), replacing E3 medium after radiation session or treated with the combination of SHD-RT (1x25Gy) and FOLFOX ChT. In this condition, after RT the E3 medium was exchanged, following FOLFOX treatment in E3 for 4 consecutive days, replaced daily (radiation procedure was performed equally as described in section 2.5). Each treatment condition had the respective non-treated zPDX controls (Figure 2.3). In the end of the assay, 4dpi, the implantation

rates (%) were estimated for all experimental conditions regarding the presence or absence of tumor. Zebrafish maximum tolerated concentration was previously determined (Fior *et al.*, 2017), using the maximum patient's plasma concentration of each ChT compound as a reference (Table 5.5, in Appendix). At 4dpi, the treated and non-treated larvae were fixed in 4% FA and dehydrated with MeOH, in the following day, for posterior immunofluorescence technique and confocal analysis.

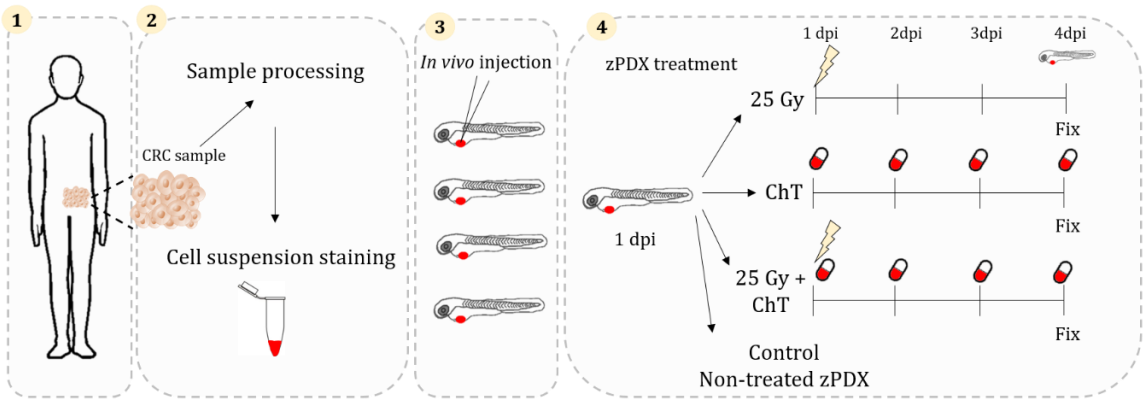

Figure 2.3. Schematic representation of zPDX experimental setup from processing to treatment. 1) Consented CRC samples resected from surgery; 2) CRC samples were processed until a cell suspension was obtained, with further cell staining; 3) Cell suspension was injected into the PVS of hundreds zebrafish larvae with 2dpf, generating zPDX; 4) In the following day (1dpi), CRC zPDX were submitted to the recommended treatment: 25Gy (SHD-RT) delivered in one radiation session, ChT (FOLFOX or 5-FU for four successive days) or the combination of SHD-RT with FOLFOX ChT, where after radiation session was given ChT, for four consecutive days. All zPDX were fixed at 4dpi and stored until perform immunofluorescence technique.

2.7 *In vivo* whole mount immunofluorescence

In the first day of the immunofluorescence staining, the zebrafish xenografts larvae and zPDX were rehydrated in methanol (MeOH, Fisher Chemicals) series with a sequential decreasing of MeOH percentage (75%, 50%, 25% in 1x DPBS) (this step was only performed when larvae were stored in MeOH). Then, larvae were permeabilized with DPBS Triton 0.1% (2x5 minutes), followed by washing with sterile water (5 minutes) and placed at -20ºC with acetone (Fisher Chemicals) for 7 minutes. The larvae were washed with DPBS Triton 0.1% and blocked for 1 hour at room temperature in a blocking solution (bovine serum albumin (0.01g/mL, Roth, Albumin fraction V), DMSO (1vol%, Sigma, dimethyl sulfoxide hybri-max sterile D2650), Triton (0.05vol%) and goat serum (0.0225vol%, Werfen, Normal Goat Serum) in 1x DPBS). The xenografts (HCT116 cells) and zPDX were incubated for 1 hour at room temperature with the primary antibodies (dilution 1:100) in the blocking solution, and maintained overnight at 4ºC. Usually it was added ~30µL of the primary antibodies diluted in the blocking solution to each eppendorf (with 10-15 larvae each). Anti-Caspase3, derived from rabbit, for apoptotic cells staining, was the specific primary antibody used to label fluorescently either for the xenografts as for the zPDX. In addition to Anti-Caspase3, Anti-human mitochondria (Anti-hmito, derived from mouse) was also a primary antibody used for zPDX, which labeled specifically human cells mitochondria (Table 2.3). To evaluate DNA damage upon radiation, Anti-γH2AX antibody (raised in mice) (1:1000 dilution) was used.

The second day started with washing steps, first two series, for 10 minutes, and then 4 times for 30 minutes with DPBS Triton 0.1%. Then, larvae were incubated with the secondary antibodies - DyLight-650 anti-rabbit (1:400) (for xenografts and zPDX) and DyLight-488 anti-mouse (1:400) (for zPDX and DNA damage), and DAPI, for nuclei staining (1:100), both diluted in the blocking solution for 1 hour at room temperature, remaining at 4ºC overnight. In the last day, the larvae were washed with DPBS Tween 0.05% (4x15 minutes), fixed in 4% FA for 20 minutes, and washed for the last time, in DPBS Tween 0.05% (4x5 minutes). Finally, the larvae were mounted in slides with mounting media (Mowiol, Sigma), and stored at 4ºC protected from the light.

For the macrophages experiments, the antibodies used were: Anti-mCherry (1:500) as the primary antibody, raised in rabbit, labelling mCherry protein and DyLight-594 anti-rabbit (1:400) and DAPI (1:100) (Table 2.3).

Table 2.3. Specifications of the primary and secondary antibodies used.

	Antibody (Colour)	Labeled target	Source	Supplier
Primary Antibodies	Anti-Caspase3 (1:100 dilution)	Apoptotic cells	Rabbit polyclonal	Cell signalling
	Anti-Mitochondria (1:100 dilution)	Nonglycosylated protein component of mitochondria of human cells	Mouse monoclonal	Merck Millipore
	Anti-γH2AX (serine 139) (1:1000 dilution)	Phosphorylated γH2AX	Mouse monoclonal	Merck Millipore
	Anti-mCherry (1:500)	Fluorescent mCherry protein	Rabbit polyclonal	Abcam
Secondary Antibodies (1:400)	Anti-rabbit (Cy5,red)	Rabbit IgG	Goat	DyLight, Thermo Fisher Scientific
	Anti-mouse (green)	Mouse IgG	Goat	DyLight, Thermo Fisher Scientific
Direct staining	DAPI (blue)	Nuclei	-	Invitrogen

2.8 Confocal microscopy of zebrafish xenografts and zPDX

All xenografts and zPDX images were acquired in Zeiss LSM 710 fluorescence confocal microscope with 5µm interval between each z-stack image. The images were analyzed in ImageJ software and quantified by counting manually, cell-by-cell, the DAPI number, mitotic figures and activated Caspase3, using Cell Counter plugin. For HCT116 xenografts, to quantify the number of DAPI for each tumor, three z-stacks (z-top, z-middle and z-last) were counted individually and then Equation 5 was applied (the equation was developed previously by the laboratory group, where the constant 1.5 used is due to previous observations that between two slices there was a common share of half of the

cells from the following slice). The mitotic figures (in the different stages of mitosis) and activated Caspase3 were counted in all tumor slices acquired, given the low readouts number per xenograft. In order to easily compare the Caspase3 quantifications made from distinct individual tumor, it was divided by the total DAPI number × 100 (percentage). It was also evaluated the effect of radiation in nuclear area size, by measuring the tumor's area, by drawing a region of interest (ROI) surrounding the tumor, and then diving it by the total number of DAPI (Equation 6). For zPDX quantifications, activated Caspase3 was counted and divided by the total DAPI number counted for all tumor z-stacks.

Equation 5. $$\text{Total cell number} = \frac{\text{AVG DAPI number}}{3} \times \frac{\text{Total slices number}}{1{,}5}$$

$$\text{Total cell number} = \frac{(\text{ztop}+\text{zmiddle}+\text{zlast})}{3} \times \frac{(\text{zlast slice} - \text{ztop slice}\,)+1}{1{,}5}$$

Equation 6. $$\text{Nuclear area size} = \frac{\left(\frac{\text{ztop ROI}}{\text{ztop DAPI number}} + \frac{\text{zmiddle ROI}}{\text{zmiddle DAPI number}} + \frac{\text{zlast ROI}}{\text{zlast DAPI number}}\right)}{3}$$

Regarding the macrophages experiments (Mpeg and Mpeg:TNFα transgenics), the macrophages in red, TNFα signal in green, and the M1-like macrophages in yellow, colour derived from the red and green overlap, were analyzed also in ImageJ and quantified manually for all z-stacks using Cell Counter tool. To calculate the number of macrophages per tumor area, the total number of macrophages were divided by the average of three tumor area size (ROI, obtained with the Measure tool). To analyse macrophages morphology in the total of experimental conditions, ImageJ was also used. Approximately 10 cells stained in red were traced and morphologically measured using the Measure tool. The parameters used to analyse the individual macrophages morphology were: Area (μm^2); Circularity, where the 1.0 value indicates a perfect circle, while values closer to 0 corresponds to macrophages with elongated and stellated (dendritic) shapes; and Perimeter (μm): the total length of a line delimitating the outside of the individual macrophages.

2.9 Statistical analysis

Statistical analysis was performed using the GraphPad Prism software (v. 7 for Windows). With exception of senescence associated β-galactosidase results that were submitted to the Fisher's exact test (Chi-square) and the survival of larvae percentages (Chi-square test), all data were challenged by two normality tests: the D'Agostino & Pearson normality test and the Shapiro-Wilk normality test. The Gaussian distribution was assumed only for datasets that pass the two normality tests and were analyzed by unpaired *t* test. Datasets that did not pass the normality test were analyzed by the Mann-Whitney test. Differences were considered significant at $P<0.05$.

2.10 β-galactosidase assay

Cellular senescence was analyzed in zebrafish xenografts of all treated conditions (Control, 5x5Gy and 1x25Gy). The larvae were fixed in FA 4% overnight. In the following day, they were permeabilized with DPBS Triton 0.1% (2x5 minutes), followed by 4 series (15 minutes/serie) of DPBS

pH7.4. Then, to decrease the pH to 6 (pH where β-galactosidase of senescent cells is activated) it was rinsed 3 times and incubated, for 1 hour at 4ºC, in DPBS pH6. After that, zebrafish larvae were transferred to 37ºC (β-galactosidase enzyme optimal temperature) overnight, in the staining solution (5mM potassium ferrocyanide, 5mM potassium ferricyanide, 2mM $MgCl_2$ and 1mg/mL X-gal diluted in DPBS pH6). When the spinal cord of zebrafish xenografts turned blue (indicative that the reaction achieved saturation), the enzymatic reaction was stopped by washing the larvae with DPBS Tween 0.05% (4x15 minutes). Before the acquisition of the images in Zeiss stereoscope, they were fixed in FA 4% and washed in DPBS Tween 0.05% (4x5 minutes). The zebrafish senescent phenotype was scored regarding the intensity of the blue colour: light blue (less senescent cells) and dark blue (high senescent cells number).

3. Results

3.1 Optimization of Neoadjuvant Radiotherapy protocol: Single-High Dose Vs Fractionated Radiotherapy

Radiotherapy (RT) is used in rectal cancer to reduce tumor burden before surgery as a Neoadjuvant (NA) treatment (Gash *et al*., 2017). Fractionated RT (FRT, 5x5Gy) or combination of FRT with Chemotherapy (ChT) are the recommended NA treatment approach given routinely in the clinic for rectal patients. NA provides the ideal setting to test the predictability of the zebrafish model for personalized medicine, in a controlled time window to access response in patients. Previous laboratory studies adapted a RT protocol to test this NA treatment in zebrafish xenografts. These results showed the ability of the adapted 1x25Gy RT protocol to distinguish radiosensitive CRC zebrafish xenografts from radioresistant ones (Figure 1.1). However, regarding our zebrafish assay, that aims a quick and feasible assay, this adapted regimen (Single-High Dose RT-SHD-RT, 1x25Gy) was applied for convenient practical reasons given that radiation is delivered in a single RT session, representing a less time-consuming protocol for the Lab, but also for the RT department, where patients are treated and not always the linear accelerator nor the staff are available to irradiate the zebrafish. However, to guarantee that this SHD-RT protocol is efficient enough and can be used as a proxy to determine radiosensitivity/radioresistance, the primary goal of my Thesis was to compare for the first time in zebrafish this SHD-RT (1x25Gy) regimen with the protocol given routinely in the clinic (FRT).

3.1.1 SHD-RT induces similar tumor responses to FRT, in 6 days

To assess whether SHD-RT (1x25Gy), one single session of treatment, which delivers 25Gy radiation dose, is a suitable regimen to test radiosensitivity/radioresistance, tumor response was evaluated and compared with the FRT (5x5Gy), which delivers 5Gy radiation for five consecutive days.

To address this aim, we generate zebrafish xenografts by using the radiosensitive CRC cell line (Xiao *et al*., 2016) HCT116 *KRAS*^{G13D}, with the *KRAS* oncogene mutated, isolated from a primary colorectal carcinoma. HCT116 cells were labeled in red with the lipophilic dye DiI and injected into the PVS of 2dpf zebrafish. On the following day, all xenografts were screened for the presence of successfully injected cells and were randomly distributed in the three experimental conditions: Control (non-irradiated xenografts), 5x5Gy (FRT), and 25Gy (SHD-RT), irradiating the xenografts in the linear accelerator in the corresponding days (Figure 3.2A). At 6 days post-injection (dpi), xenografts were fixed and processed for confocal microscopy analysis (Figure 3.2B-M).

However, before accessing the anti-tumoral effects of RT, we also evaluated the radiation impact in zebrafish larvae mortality. The survival Kaplan-Meier curve in Figure 5.1 (Appendix) showed that more than 75% of larvae survived until the end of the assay (6dpi). Nevertheless, the FRT irradiated xenografts (5x5Gy) showed a higher percentages of mortality (25%) compared to the Control (14.19% death, **P*=0.0368) and to the SHD-RT (1x25Gy) (8% death, ***P*=0.006).

Radiation can induce cellular damage acting directly on the genetic material. DNA double strand breaks (DSB) represents the most lethal injury caused by ionizing radiation (IR), and in response

to the damage several mechanisms and proteins are activated in order to repair the DNA (Baskar *et al*., 2014). γH2AX, a histone present in the nucleosomes is phosphorylated upon damage in serine 139 residue, constituting a useful indicator of DSB formation (DNA damage) (Pouliliou and Koukourakis, 2014). Thus, in order to confirm the direct DNA injury triggered by the radiation doses given to the CRC xenografts, we performed an immunofluorescence against γH2AX. Irradiated xenografts with 5Gy and 25Gy doses were fixed 1 hour-post radiation (hpr) and compared to controls. Our results confirmed the induction of damage by radiation in both doses, with a clear stronger induction in the SHD-RT (25Gy) due to the delivered high dose (Figure 3.1A-C).

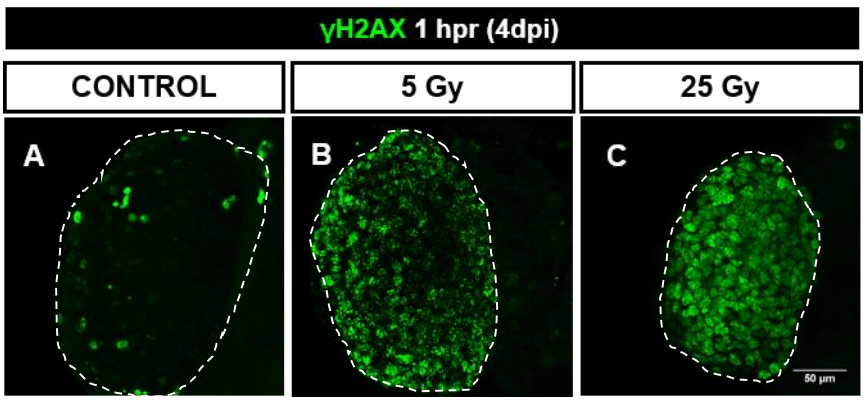

Figure 3.1. Radiation induced DNA damage. At 4dpi, CRC xenografts (HCT116) were irradiated with 5Gy and 25Gy doses, and fixed 1 hour after radiation. Phosphorylated γH2AX (in green) as a marker of DNA damage was detected by immunofluorescence in all experimental conditions (Control, 5Gy and 25Gy); A-C confocal microscopy images are in the same magnification (25x objective). Tumor area is delineated by a dashed and white line. Scale bar (50µm).

Next, we analysed the impact of both protocols in the tumoral biologic response. First, we analysed radiation effect on proliferation by quantifying mitotic figures. Irradiated tumors showed a significant reduction in the percentage of mitotic figures (****P<0.0001; Control AVG = 0.42, 5x5 Gy AVG=0.04; 25 Gy AVG=0.12) in relation to the controls, representing more than 90% reduction in FRT xenografts and a 72% decrease in SHD-RT (Figure 3.2N).

Additionally to cell division impairment, RT achieves its therapeutic effect by triggering cell death, further hindering tumor progression. Since apoptosis represents one of the major types of cell death activated by IR (Baskar *et al*., 2014) we evaluated the impact on apoptosis of the CRC cells. Thus, the presence of activated Caspase3, a protein involved in the apoptotic signalling cascade, was quantified (Figure 3.2D, H, L and O). Both protocols showed a significant increase of activated Caspase3, with 2 fold increase in the FRT condition and 3 fold increase observed for SHD-RT comparing to the control (****P<0.0001). At 6dpi, SHD-RT regimen exhibited significant higher percentages of cell death by apoptosis than FRT (****P<0.0001).

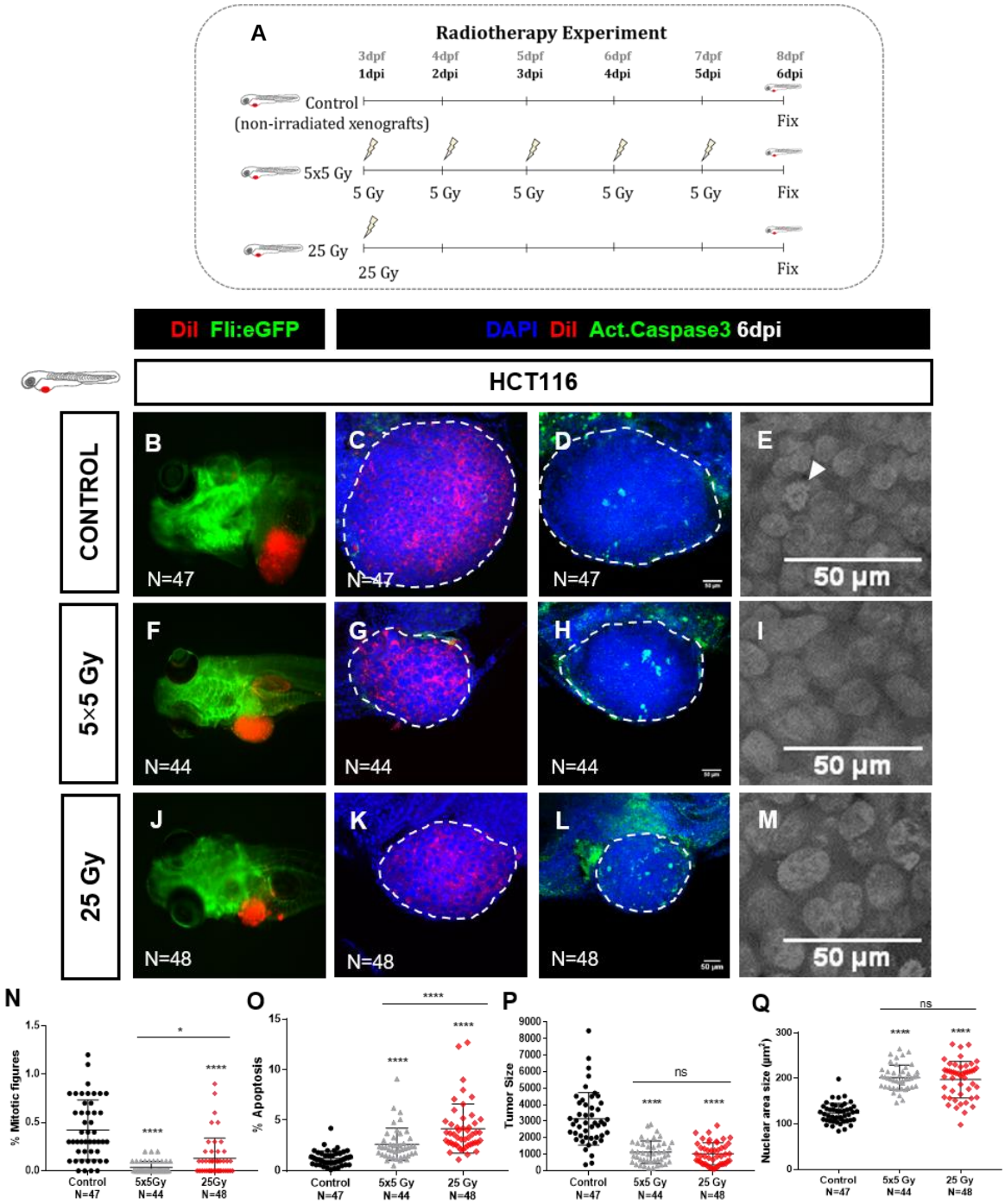

Figure 3.2. SHD-RT (1x25Gy) induces similar tumor effects to FRT (5x5Gy), in 6 days. The experimental set up is illustrated in scheme A. Human CRC zebrafish xenografts were generated by HCT116 cells (labeled with DiI dye, in red) injection into the PVS of 2dpf zebrafish. 1dpi, zebrafish radiosensitive xenografts were treated with FRT (5x5Gy) for five consecutive days (F-I) or SHD-RT (1x25Gy) in a single RT session (J-M) and then compared with non-irradiated controls (B-E). B, F and J are representative zebrafish xenografts at 6dpi for the three experimental conditions, obtained using Zeiss AxioScan Z1. Fixed zebrafish xenografts (6dpi) were analyzed and quantified for: mitotic figures (%) (N), apoptosis (%) (activated Caspase3) (O), tumor size (total DAPI number) (P) and nuclear area size (total DAPI number/tumor area size (ROI)) (Q). N-Q results are average of three independent experiments and are expressed as AVG±SD. Tumor area size is delineated by a dashed white line (C, D, G, H, K, L). The white arrowhead in E illustrates a mitotic figure. Confocal microscopy images in C, D, G, H, K, L are at the same magnification (40x) as E, I and M. Each dot represents a xenograft and the total quantified xenograft is indicated (B-Q). Mann-Whitney test was the statistical analysis used. *P value*, **P*<0.05 *****P*<0.0001; ns, nonsignificant. Scale bar (50 µm).

Importantly, this induction of apoptosis was followed by a significant tumor size reduction (>50%, *****P*<0.0001) compared to the control and no statistical differences were observed between

both radiation regimens (FRT DAPI number AVG=1120; SHD-RT DAPI number AVG: 1029) (Figure 3.2P). Another phenotype analyzed was the nuclear size, since it has been described that IR due to chromatin modifications increases the size of the nuclei (Maier *et al*., 2016).The nuclear area size was measured for the treated xenografts and compared with the respective control. As it can be observed in Figure 3.2Q, a significant, but similar increase of nuclear area was observed for both irradiation protocols (****P<0.0001; FRT AVG=202µm^2; SHD-RT AVG=197.3µm^2) comparing to the non-irradiated tumors (nuclear area size AVG=123.5µm^2) (Figure 3.2E, I, M and Q).

Overall, our results show that in 6 days both RT protocols can elicit CRC cells proliferation blockage, trigger cell death through apoptosis with a subsequent clear reduction on the tumor size. Moreover, the nuclei enlargement observed in cancer cells is consistent with the described radiation effect in chromatin (Maier *et al*., 2016), and it also suggested to be an indicator of radiosensitivity. Thus, our data suggests that the SHD-RT (1x25Gy), for convenient and time-consuming practical purposes, is an appropriate and efficient regimen to discriminate CRC radiosensitive zebrafish xenografts.

Apoptosis is the predominant cell death type elicited by IR (Baskar *et al*., 2012), however radiation-induced stress and exposure to DNA damage can also lead to cellular senescence. Senescence is characterized by cell cycle arrest and one of its hallmarks is an excess of lysossomal β-galactosidase activity at pH6 (Collado and Serrano, 2006). Thus, to address the senescent phenotype after RT, a β-galactosidase assay was performed, at 6dpi. This cytochemical assay allows the detection of β-galactosidase activity using the chromogenic substrate 5-bromo-4chloro-3-indolylβ-D-galactopyranoside (X-Gal) which turns into blue after the β-galactosidase lysosomal activity. Xenografts from all treatment groups were scored according to staining intensity, where dark blue tumors were indicative of higher number of senescent cells, while light blue tumors had less senescent cells. The results revealed no significant differences between the control and both treatment groups (P=0.5161), where in all three experimental conditions was observed high percentages of zebrafish larvae xenografts with strong senescent phenotype (>77%), suggesting that HCT116 cells senescence is not influenced by IR (Figure 3.3C).

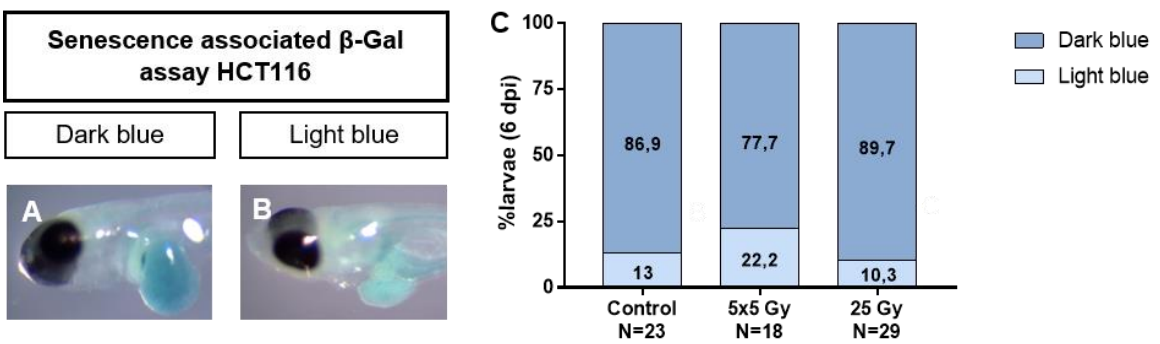

Figure 3.3. CRC irradiated xenografts did not show alterations in senescence associated β-galactosidase upon different RT protocols. 3dpf zebrafish xenografts (HCT116 radiosensitive cells) were irradiated with FRT and SHD-RT protocols and compared with the respective non-irradiated controls. In the end of the experiment (6dpi), the xenografts were submitted to β-galactosidase assay. CRC xenografts senescence was analyzed by scoring tumors according to blue staining intensity: dark blue represents xenografts with high number of senescent cells (A); and light blue indicates xenografts with few senescent cells (B). The percentage of senescence xenografts larvae are represented in C, as well the total number of analyzed zebrafish. The statistical analysis was performed using the Fisher's exact test (Chi-square), however no significant differences were observed.

3.1.2 Time is determinant for the cumulative FRT anti-tumoral therapeutic effects

Although we observed similar impacts on tumor downsizing in both protocols, we saw a higher induction of apoptosis in the SHD-RT protocol than in the FRT. However, the overall time after SHD-RT ending (5 days-post treatment – dpT) was not the same time given to the total FRT dose (1 day after the last treatment), raising the question whether time after treatment was determinant for RT to elicit its anti-tumoral therapeutic effects, and whether we were missing effects from the FRT? In other words does "time matters"?

Thus, to address this question we designed an experiment where the exact same time after treatment (3dpT) was given for both RT protocols. As described previously, HCT116 zebrafish xenografts were generated and at 1dpi were randomly distributed into the different experimental conditions: Control (non-irradiated xenografts), FRT protocol (5x5Gy) and SHD-RT (1x25Gy) (Figure 3.4A). Following 3 days-post RT, tumor response was evaluated and both protocols were compared between them and to their respective controls (Figure 3.4F-I). The comparison between the two RT regimens (now given a total of 3 days after treatment in both) revealed that both led to a decrease in mitotic figures (FRT: 61% reduction, **P*=0.0194; SHD-RT: 88% reduction, *****P*<0.0001) (Figure 3.4F). However, only the SHD-RT (4dpi – 3dpT) showed high levels of apoptosis either when compared to its respective 4dpi control (***P*=0.0018, 2 fold increase) or to the FRT (8dpi – 3dpT; **P*=0.0380) (Figure 3.4G). Despite the non-statistical differences for cell death at 3 days after FRT, a clear tumor mass reduction was observed compared to the respective (80% reduction, *****P*<0.0001), suggesting that the peak of apoptosis occurred earlier. A significant reduction of tumor size was also observed for SHD-RT (59% reduction, *****P*<0.0001) compared to its control. However at 3dpT the fractionated protocol exhibited stronger anti-tumoral effects regarding tumor size decrease than the SHD-RT (****P*=0.0007) (Figure 3.4H). Nuclear area size was also analyzed and our results show that both RT protocols induced the enlargement of HCT116 cells nuclei (*****P*<0.0001), however, the effect was superior in FRT, with high statistical differences when compared to the SHD-RT (AVG=1.92 Vs AVG=1.41 fold increase, respectively) (*****P*<0.0001) (Figure 3.4I).

Thus, our data revealed that giving the same overall time after RT treatment for the two radiation protocols, the cumulative fractions of FRT (5x5Gy) exhibited a stronger effect in decreasing tumor size as well in increasing nuclear area size. These results, show that cumulative damage and time are crucial factors for the radiobiology of FRT tumor response.

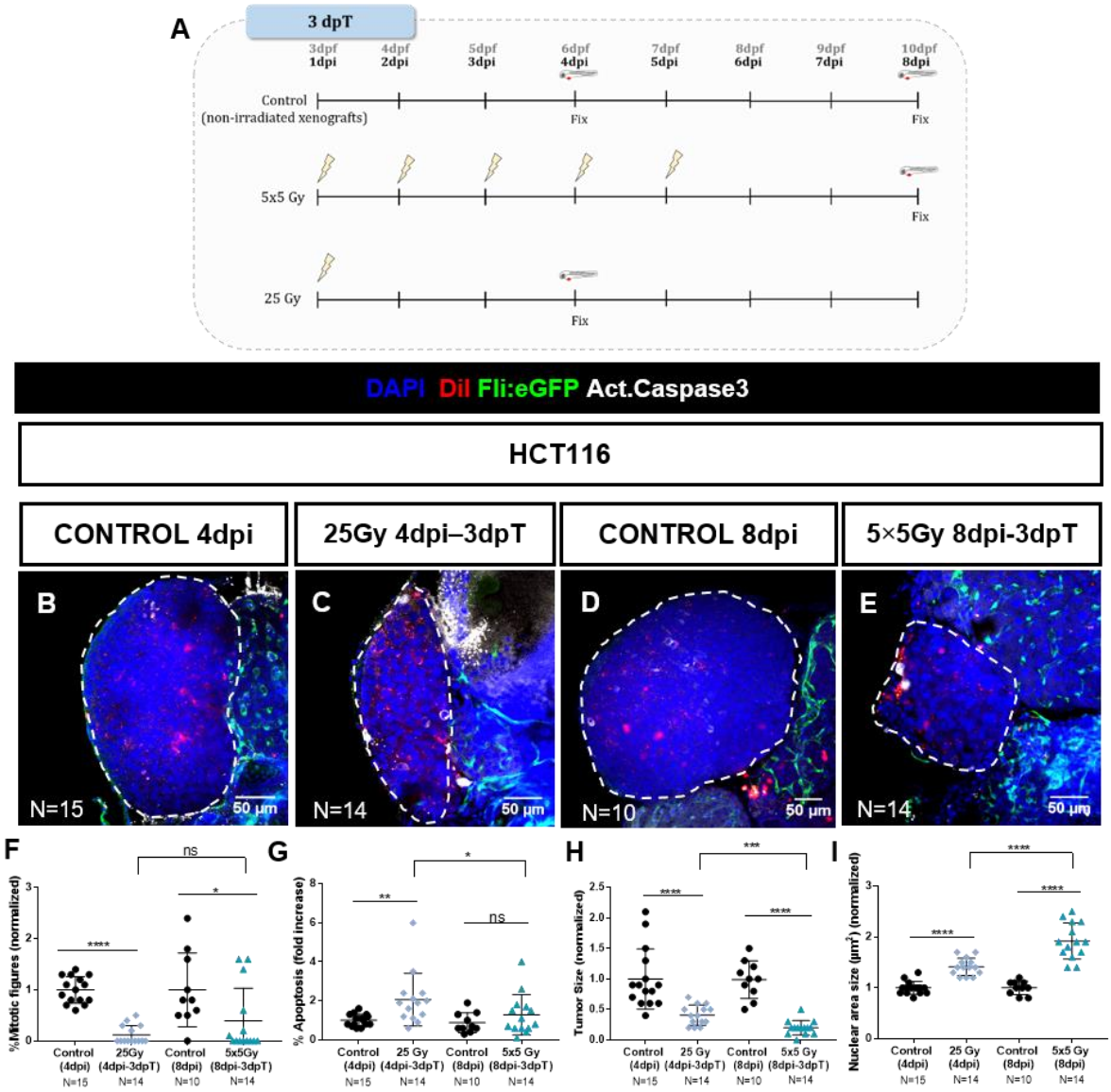

Figure 3.4. FRT elicits stronger tumor response than SHD-RT, after 3 days of treatment ending. The experimental set up is represented in scheme A. CRC-xenografts were submitted to FRT (5x5Gy) and SHD-RT (1x25Gy) protocols and compared with the controls (non-irradiated xenografts). In order to evaluate both RT protocols tumor effect with the same overall time after treatment ending (3dpT), SHD-RT xenografts were fixed at 4dpi and the FRT irradiated zebrafish were fixed at 8dpi. The respective non-irradiated controls were also fixed (4 and 8dpi). All the fixed xenografts were analyzed and quantified for: mitotic figures (%) (F), apoptosis (%) (activated Caspase3) (G), tumor size (total DAPI number) (H), and nuclear area size (total DAPI number/tumor area size (ROI)) (I). Results in F-I are normalized to the respective controls, where each dot represents a xenograft from an individual experiment. F-I results are expressed as AVG±SD. *P values*, **P*<0.05, ***P*<0.01,****P*<0.001 and *****P*<0.0001; ns, nonsignificant. The statistical analysis was performed using Mann-Whitney test. Total number of analyzed xenografts are indicated (B-I). HCT116 cells are stained in red (DiI dye), nuclear DAPI in blue. B-E confocal images were taken with 25x objective and the white dashed line is defining tumor size. Scale bar (50µm).

To further compare the time after treatment we normalized data to the respective controls (Figure 3.5). Increasing time after FRT (3dpT), showed a notable tumor reduction of 80%, more than the observed at 1dpT (68% reduction) (****P<0.0001) revealing that time is essential for the cumulative fractions anti-tumoral effects, which exhibit stronger tumor responses than SHD-RT (Figure 3.5C). Our

results also suggested that SHD-RT requires more time after treatment to elicit similar tumor responses to FRT (FRT 3dpT Vs SHD-RT 5dpT), showing the relevance of time increase in apoptosis.

Interestingly, increasing time after radiation revealed a significant enlargement of HCT116 nuclei size for the FRT condition (3dpT), even more than the increase observed at 1dpT (HCT116_nuclear area size ((5x5Gy: 1dpT Vs 3dpT), ***P*=0.0045). In opposition, time did not influenced HCT116 nuclei dimensions submitted to the SHD-RT protocol (Figure 3.5D).

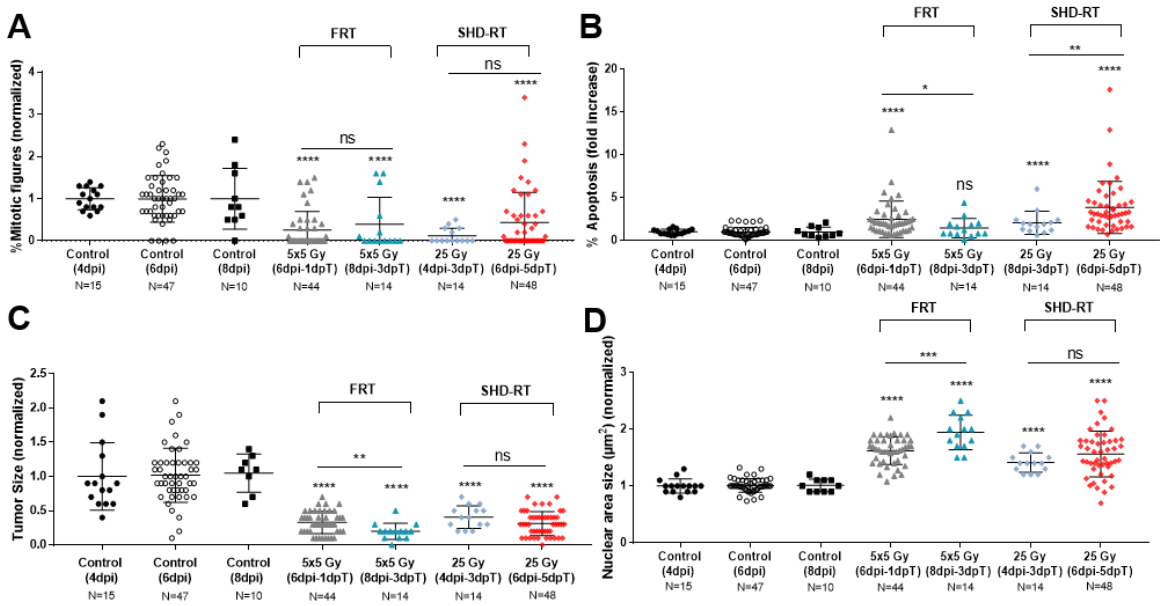

Figure 3.5. Time is determinant for the radiobiology of cumulative daily fractions of FRT. Statistical results in Figure 3.2N-Q were normalized to the respective controls and compared with the results in Figure3.3F-I. A-D results are from two independent experiments, where each dot indicates one xenograft analyzed. Xenografts total number are indicated in A-D. ns, nonsignificant; *P values*, **P*<0.05, ***P*<0.01, and *****P*<0.0001. Mann-Whitney test was performed for the statistical analysis.

In summary, our data suggested that "time matters". Our findings showed that the tumor biological effects elicited for FRT protocol is time-dependent, increasing with time. The comparison of the two RT regimens with the same time after treatment ending showed that the cumulative FRT protocol is more efficient hindering tumor development than SHD-RT, i.e. the cumulative effect, of imposing repetitive damage to a tumor is more effective than a Single-High Dose.

The impact of time in tumor response following RT, prompt us to further challenge time after treatment. Instead of an overall time of 3 days (3dpT), 1 day after RT (1dpT) was given for both RT protocols (FRT and SHD-RT). Following 1dpT, irradiated xenografts as well the respective non-irradiated xenografts (controls) were fixed (Figure 3.6A), analysed in confocal microscopy and quantified. Our data showed that significant reduction in mitotic figures in both RT conditions (>87% reduction, SHD-RT ****P*=0.0003; FRT *****P*<0.0001) compared to the control (Figure 3.6F). Although we could not observe an induction of apoptosis, FRT induced a clear tumor mass decrease (>67% reduction, ****P*=0.0002) (Figure 3.6G), as well the enlargement of the nuclei were observed (*****P*<0.0001) (Figure 3.6H). Regarding SHD-RT regimen, despite proliferation impairment and apoptosis induction, no significant differences were detected in tumor size after 1 day of RT (Figure 3.6F-H). Thus, our results highlight once more the "time" as a critical factor for a clear tumor response,

as well the stronger effect of FRT than SHD-RT, with the same interval time after treatment. These results also showed that time is important in tumor response to SHD-RT, where increasing time after RT from 1dpT to 3dpT led to a stronger anti-tumoral effect.

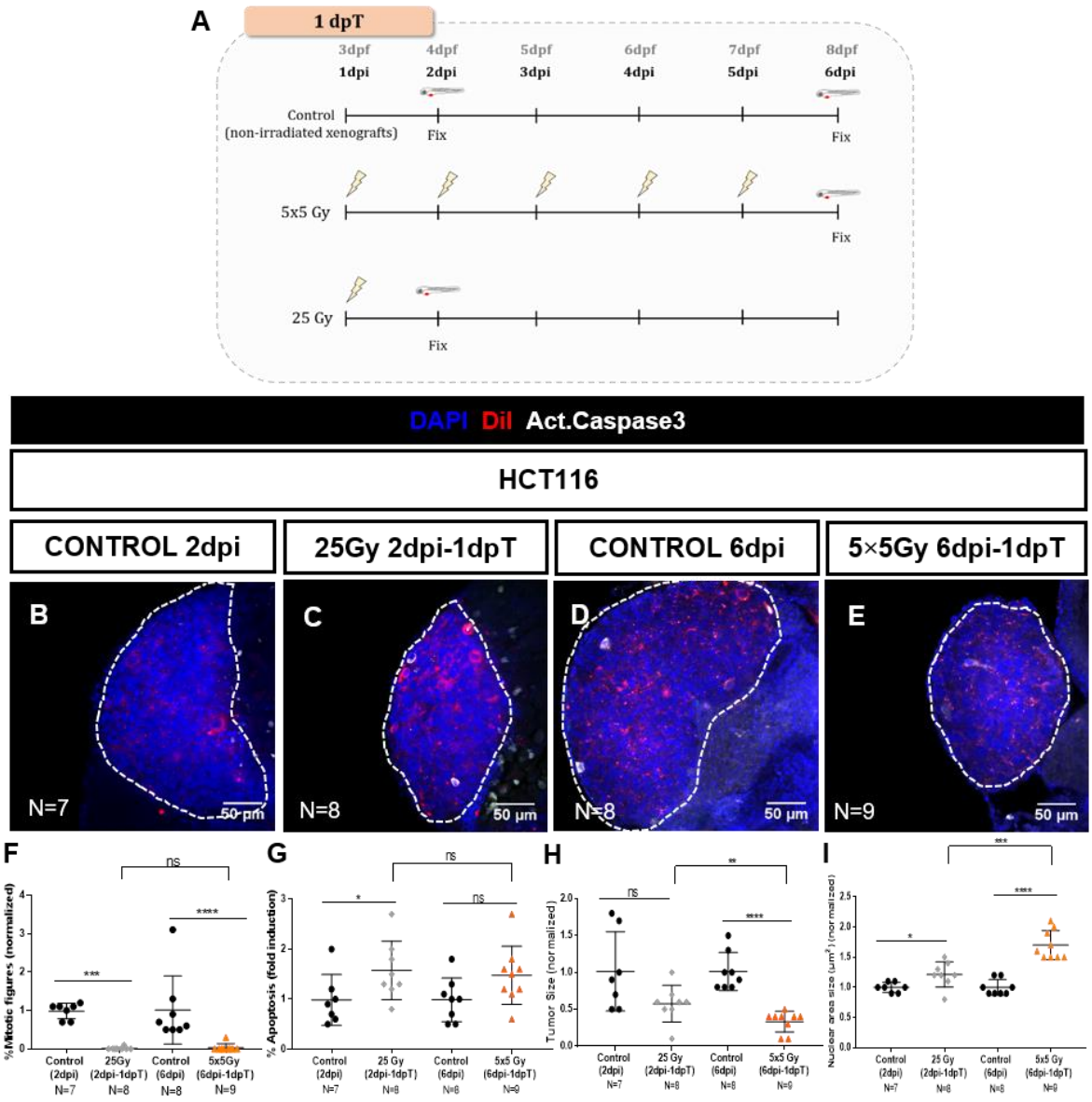

Figure 3.6. Time following RT is determinant for a more effective tumor response. Schematic representation of RT regimens given to CRC zebrafish xenografts (A). At 1dpi, the CRC xenografts were randomly divided into the three experimental conditions: Control (non-irradiated xenografts); FRT (5x5Gy); and SHD-RT (1x25Gy). SHD-RT and FRT xenografts were fixed at 2dpi and 6dpi, respectively, performing both 1dpT, and compared with their respective controls. Mitotic figures (%) (F), apoptosis (%) (activated Caspase3) (G), tumor size (total DAPI number) (H), and nuclear area (total DAPI number/tumor area size (ROI)) (I) were analyzed and quantified for all experimental groups. F-I results are normalized to the respective controls and each dot corresponds to an individual xenograft from one independent experiment. ns, nonsignificant; *P values*, **P*<0.05, ***P*<0.01, ****P*<0.001 and *****P*<0.0001. Results are expressed as AVG±SD (F-I) and the number of xenografts analyzed are indicated. Dashed white line is delimiting tumor size from B to E, images with the same magnification (25x objective). Scale bar (50µm).

Additionally, we tested whether the age of the xenografts could influence tumor response to RT, as a "tumor" consequence, maintaining the overall time following treatment ending.

Once again radiobiology was evaluated and compared between both RT regimens (FRT and SHD-RT) with an overall time of 3 days (Figure 3.7E-H) after therapy. However the SHD-RT (1x25Gy) dose was delivered at 5dpi, in opposition to FRT regimen that started at 1dpi (Figure 3.7A). Once more, our data showed that the daily 5Gy fractions elicit a stronger therapeutic effect compared to the 25Gy Single-High Dose, regarding tumor reduction (***P=0.0003). These results also suggested that independently on the irradiation day (for SHD-RT), FRT effectiveness is superior to SHD-RT.

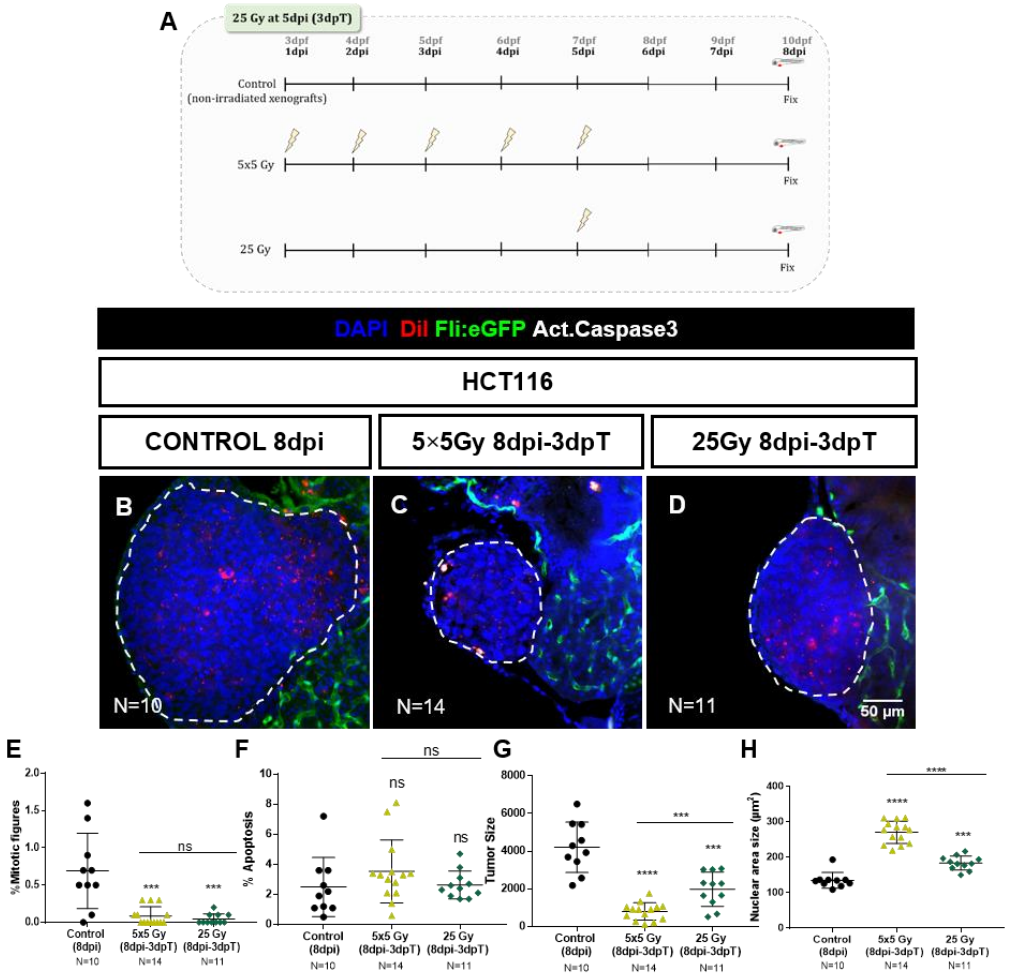

Figure 3.7. Independently of irradiation time point, FRT is more effective than SHD-RT, with the same overall time following treatment ending. The CRC-xenografts (at 1dpi) were divided in the experimental conditions: Control (non-irradiated xenografts); FRT (5x5Gy) starting treatment at 1dpi; and SHD-RT (1x25Gy) irradiated only at 5dpi. The irradiated xenografts were then fixed at 3dpT (8dpi), as well the respective controls (illustrated in A). All xenografts were analyzed and quantified for: mitotic figures (%) (E), apoptosis induction (%) (activated Caspase3) (F), tumor size (total DAPI number) (G), and nuclear area size (total DAPI number/tumor area size (ROI)) (H). The total number of analyzed xenografts is indicated (B-H). E-H results are from one independent experiment, where each dot represents one xenograft. With exception of tumor size results (G), where a Gaussian distribution was assumed, E,F and H results were submitted to Mann-Whitney test as the statistical analysis. ns, nonsignificant; *P values*,***P<0.001, ****P<0.0001. Results are expressed as AVG±SD (E-H). Confocal microscopy images (B-D) were taken with a 25x objective, Scale bar (50µm).

Given that HCT116 tumors irradiated at 5dpi had more time to adapt and proliferate before treatment, having time to approximately double the size of 1dpi xenografts (Figure 6.2 in Appendix), we asked whether tumor size influences RT efficacy. Therefore, results of SHD-RT irradiation at 1dpi (Figure 3.6F-I) and 5dpi (Figure 3.7E-H), with the same overall time following RT (3dpT), were compared (Figure 3.8A-D). Interestingly, our results show that SHD-RT was able to elicit a similar tumor response regardless of the initial tumor size.

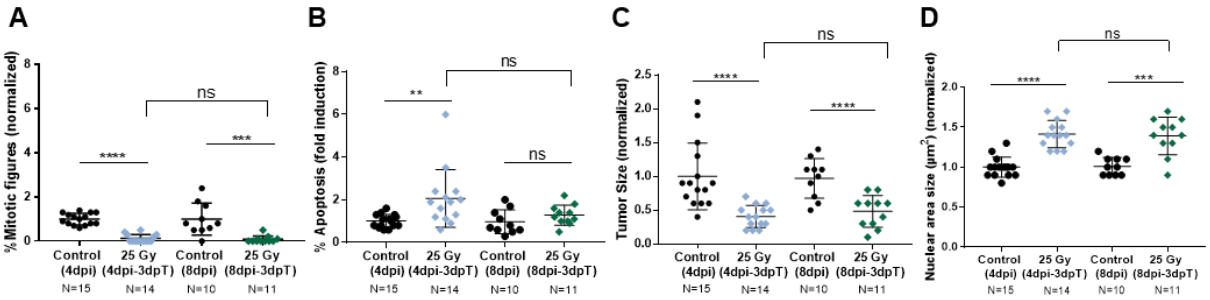

Figure 3.8. CRC xenografts tumor size did not influence SHD-RT tumor response. The results obtained for 25Gy from Figures 3.6 and 3.7 were normalized and compared to the respective controls. The mitotic figures (%) (A), apoptosis (%) (activated Caspase3) (B), tumor size (C) and nuclei dimensions (D) were the analyzed biological features. The results are the average of the different experimental conditions evaluated (AVG±SD). The total number of analyzed xenografts is indicated (A-D). A-D results are from two independent experiments, where each dot represents one xenograft. ns, nonsignificant; *P values* ***P*<0.01; ****P*=0.001; and *****P*<0.0001. Mann-Whitney test was the performed statistical analysis.

3.10 CRC zebrafish Patient-derived Xenografts

The ultimate goal of the Lab is to develop a drug screening platform using zebrafish as the *in vivo* model, to assess tumor response to the recommended treatments to then help tailor treatments for each individual patient. Recently, our Lab showed the possibility to assess CRC zebrafish Patient-derived Xenograft (zPDX) responses to Adjuvant Chemotherapy (ChT), as a proof-of-principle with promising results. However, the predictability of the model needs to be further tested with more samples, as well in a more controlled setting, as NA setting, where the effects of therapy can be quantified in a more accurate manner in a short time window.

Thus, the lab team work is focused on improving the zPDX protocol and testing the recommended therapies for colorectal and breast cancer, where I also participated besides my main goal on comparing both RT protocols. The main tasks that I was involved were:

- Receiving CRC consented samples from Amadora Sintra Hospital and Champalimaud Foundation and process them for cryopreservation;
- Helping in sample processing for injection - where tissue was dissociated, and the resulting cell suspension was stained with a lipophilic dye (DiI) to inject;
- And injection into the PVS of a 2dpf zebrafish, generating CRC zPDX.

Since I was developing and testing the RT protocol with CRC cell lines to be applied zPDX NA setting, we tested for the first time this SHD-RT (1x25Gy) protocol in zPDX. These were samples, whose patients did not receive any treatment and therefore could not be used for the predictive study

and consequently they can be used for optimization of protocols. Following injection day, and in order to test tumor responses to treatment, colon and rectum zPDX were submitted to SHD-RT (1x25Gy), FOLFOX or 5-FU ChT, or SHD-RT in combination with FOLFOX, as illustrated in Figure 3.9.

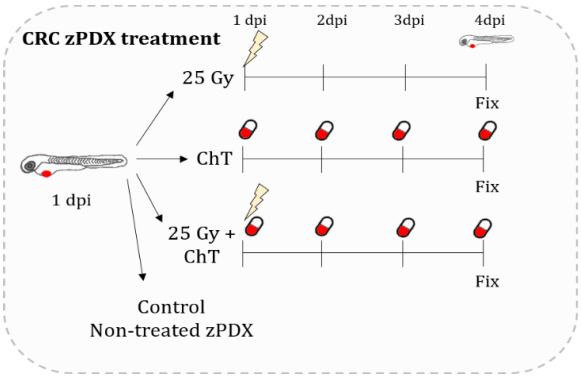

Figure 3.9. CRC zPDX treatment regimens. Following colon and rectum cell suspensions injection into the PVS of 2dpf zebrafish, the zPDX were submitted to the recommended therapy: colon zPDX (1dpi) were treated with FOLFOX ChT or 5-FU for four consecutive days, whereas rectum zPDX were submitted to RT alone (SHD-RT, 25Gy) at 1dpi, or to the combination of RT (SHD-RT, at 1dpi) with ChT (FOLFOX, for four successive days). Every treatment conditions had the respective non-treated controls. At 4dpi, all zPDX were fixed and processed for immunofluorescence assay.

At 4dpi, the presence of a tumoral mass was quantified, calculating the implantation (engraftment) percentage (Figure 3.10). These results are the sum of the work developed in the Lab over a year, mainly by Bruna Costa a Post-Doc colleague, in which I helped and participate in the experimental work. The implantation data suggested that either rectum as well as colon zPDX subjected to FOLFOX tended to exhibit variability in the engraftment rates, while the irradiated rectum zPDX suggested a possible trend to increase implantation rates compared to the respective controls (Figure 3.10B). These results possibly suggests that besides radiation anti-tumoral effects, it could also affect zebrafish microenvironment, with possible enhancement of the rectum zPDX implantation rates.

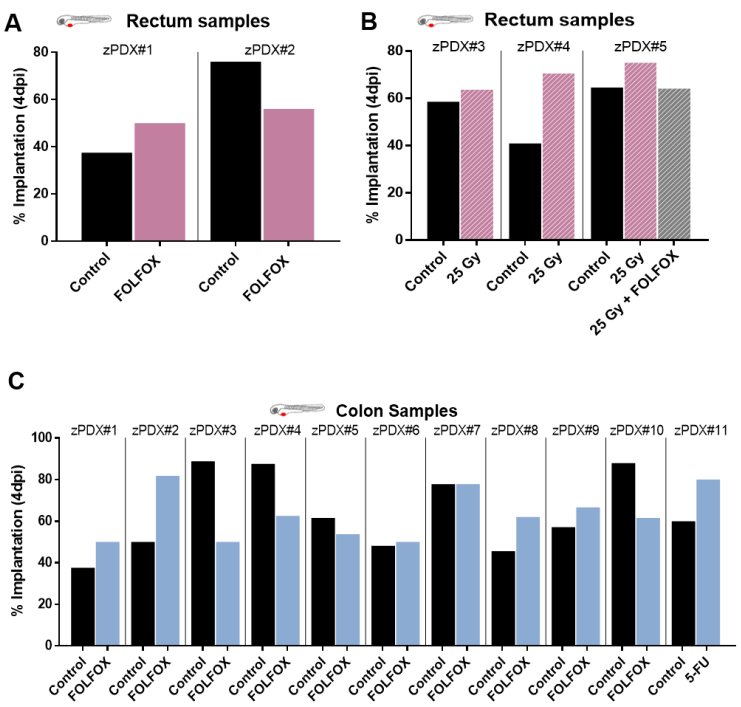

Figure 3.10. CRC implantation rates at 4dpi. Cells suspension obtained from patient surgery resected samples were injected in the PVS of 2dpf zebrafish larvae. Since day 1 post injection to 4dpi rectum (A) and colon samples (C) were submitted to FOLFOX ChT, with exception of colon zPDX#11 treated only with 5-FU (these results are the representation of the overall work developed by our Lab's team, were I was involved to help. Different rectum samples were irradiated with SHD-RT (25Gy) at 1dpi, or treated with RT (25Gy) at 1dpi and submitted to ChT (FOLFOX) for four successive days (B) (These results were obtained after guarantee that SHD-RT was enough to determine radiosensitivity. At 4dpi, zebrafish number with tumor (stained in red dye - DiI) were quantified and calculated the percentage of larvae with tumor mass. Results are represented in A-C. Each zPDX number represents distinct rectum or colon samples that were injected once, each in one independent experiment.

Then, to test the anti-tumoral effects of the corresponding treatments, CRC zPDX were analyzed at 4dpi (3dpT). Quantification of apoptosis showed that only the combination of RT (25Gy) with ChT (FOLFOX) induced significantly cell death (Figure 3.11G). In addition to activated Caspase3, human mitochondria was also labeled aiming an easier discrimination between human primary cells and the host cells. Surprisingly, confocal microscopy images suggested the presence of more positive cells for human mitochondria after RT, either alone or in combination. This possible increase in human mitochondria after RT and the slight trend in implantation rates improvement after RT, might suggests a possible immune suppression.

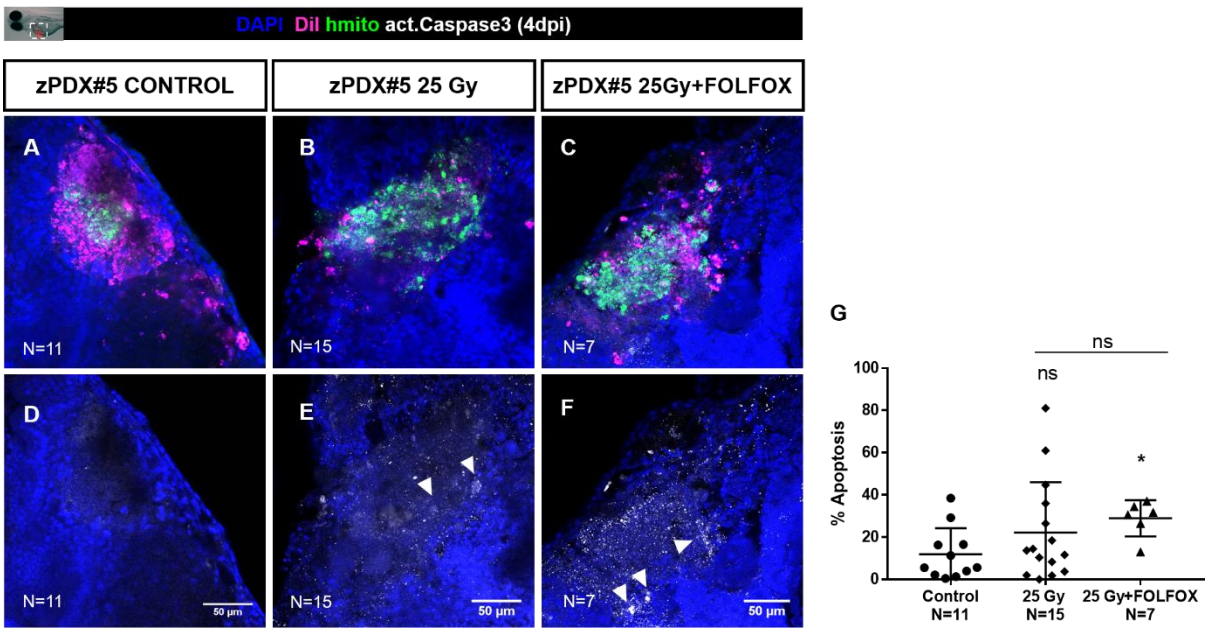

Figure 3.11. Combination of RT and ChT induces cell death in rectum cancer human sample (zPDX#5). The labeled rectum cell suspension (DiI dye, in magenta) was injected in the PVS of zebrafish (2 dpf), generating zPDX. At 1 dpi, zPDX#5 were randomly distributed in the different experimental conditions: Control (non-treated zPDX); SHD-RT (1x25 Gy); and SHD-RT combination with FOLFOX ChT, where the 1 dpi zPDX were irradiated receiving the dose in one single session of treatment, following ChT for four consecutive days. All zebrafish larvae were fixed at 4 dpi and processed for immunofluorescence assay. Fixed larvae were analyzed and quantified for apoptosis (%) (activated Caspase3) (G). Human mitochondria (hmito) was also stained in green. The results are from one independent experiment (AVG±SD), where each dot represents an individual zPDX analyzed and quantified. The total number of zPDX analyzed are indicated (A-G). The statistical analysis was performed using Mann-Whitney test. *P value*, *$P<0.05$; ns, nonsignificant. Images from the same column are ate the same magnification (25x). The arrowheads are indicating apoptotic cells. Scale bar (50µm).

3.11 Radiation decreases macrophages number in CRC xenografts

Macrophages are one of the predominant immune cells in tumor microenvironment (TME), with an important role in tumor progression and therapy response (Genard *et al*., 2017). Therefore, the increase in cells positive for human mitochondria cells, and the slight enhancement trend in the engraftment of irradiated rectum zPDX (1x25Gy), led us to question whether radiation was affecting zebrafish innate immune system, namely the macrophages (Filatenkov *et al*. 2015). For this, HCT116-CRC xenografts were generated in zebrafish transgenic with a red reporter for macrophages (mpeg1:mCherry). Following injection day, xenografts were irradiated with a single dose of 25Gy (SHD-RT) and further fixed at 4dpi and 6dpi, to quantify the number of macrophages cells surrounding the tumor (Figure 3.12G-J). Confocal images showed that macrophages were mainly present in tumor periphery, with only a few cells infiltrating the tumor (Figure 3.12A-F).

Quantification of the number of macrophages in the tumor area revealed a significant reduction of their total upon radiation, with a higher reduction at 6dpi (76% reduction, ****P<0.0001) compared to 4dpi (62% reduction, ***P=0.0001) (Figure 3.12G and I, respectively). Thus, these preliminary results revealed that radiation reduces the number of macrophages, which may contribute to favor the engraftment of rectum zPDX (observed in Figure 3.10B), as well an enhancement of human mitochondria signal at 4dpi (Figure 3.11).

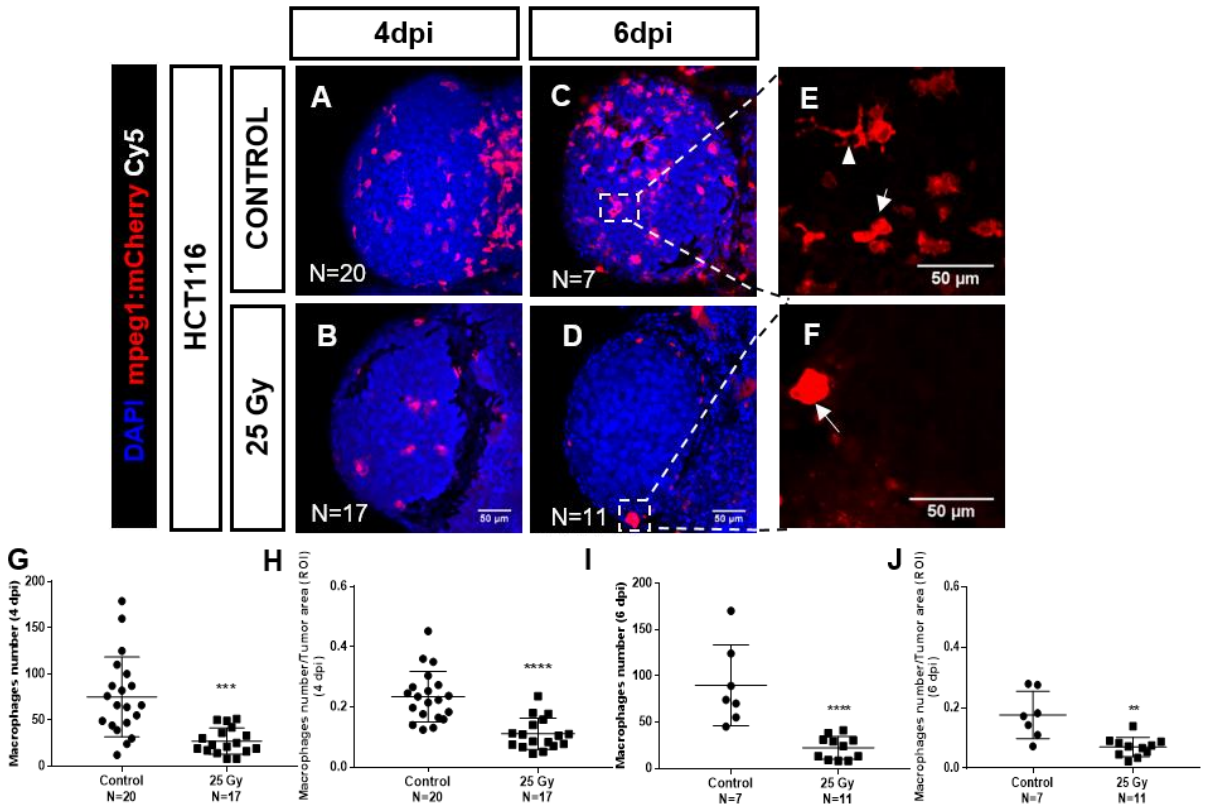

Figure 3.12. SHD-RT decreases macrophages number in the tumor area, until 6dpi. HCT116 cells (labeled with Cy5 dye) were injected into the PVS of 2dpf zebrafish mpeg1:mCherry transgenic. Following the injection day, CRC xenografts were irradiated with SHD-RT regimen (1x25Gy) and fixed at 4dpi or at 6dpi. For both time points, the macrophages were analyzed and quantified: G and I graphics represent the overall of macrophages number present in the tumor site, while H and J are the values obtained for macrophages number per tumor area size (ROI). Results are expressed as AVG ± SD (G-J). Statistical analysis was performed using Gaussian distribution (G) and Mann-Whitney test (H-J). *P values*, ***P*<0.01; ****P*=0.0001; and *****P*<0.0001. Total xenografts analyzed are represented in G-J. A-D are confocal microscopy images obtained with a 25x objective: the nuclei are stained in blue (DAPI) while macrophages were labeled in red (mCherry antibody). E and F are at the same magnification and represent a zoom in of C and D, respectively. E and F show the different macrophages morphologies observed: white arrowhead represents dendritic/stellate macrophages, whereas the white arrow illustrate the rounded innate immune cells. Scale bar (50µm).

3.12 M1- and M2-like macrophages exhibit high heterogeneity in morphology with no correlation between shape and function

Macrophages are one of the major players of the TME but presents a highly heterogenic phenotype. Their plasticity relies on their two "main" opposite functions / states: M1-like, the pro-inflammatory macrophages - associated with an anti-tumoral activity; and M2-like macrophages, influencing positively tumor development (pro-tumoral). Moreover, radiation is known to modulate macrophages polarization towards a M2-like phenotype (Genard *et al*., 2017). In order to test whether radiation impacted on macrophage phenotype we analyzed M1-like macrophage phenotype in irradiated CRC (Figure 3.13). Once more HCT116-CRC xenografts were generated, but now using as host a reporter zebrafish transgenic line that labels macrophages in red and Tumor Necrosis Factor Alpha (TNFα) in green (mpeg1:mCherry-F/ tnfα:eGFP-F), one of the pro-inflammatory molecules responsible for M1-like activation, which is also expressed by these macrophages (Genard *et al*., 2017). At 1dpi, CRC xenografts were irradiated (SHD-RT, 1x25Gy), and fixed at 4dpi, analyzing and quantifying the following cells (Figure 3.13E, G):

- The total number of macrophages, labeled in red ($mpeg^+$);
- The total inflammatory cells expressing TNFα ($tnf\alpha^+$) in green, including the anti-inflammatory macrophages (M1-like);
- The percentage of double positive cells i.e. $mpeg^+tnf\alpha^+$, in yellow (considered the M1-like macrophages, that for simplicity was named "M1") ;
- The percentage of $mpeg^+tnf\alpha^-$ (considered the M2-like macrophages that also for simplicity was denominated by "M2").
- And the percentage of inflammatory cells expressing TNFα that are not macrophages i.e ($mpeg^-tnf\alpha^+$);

Again, radiation revealed a capacity to decrease the total macrophages number (67% reduction, ***P*=0.0078) but also showed to reduce the total number of TNFα inflammatory cells (78%, ****P*=0.0002) (Figure 3.13E). Despite the reduction observed in the total number of macrophages no significant differences were observed in the average percentage of M1-like or M2-like (AVG: 57% and 43%, respectively) compared to the respective controls (AVG: 51% and 48%, respectively) (Figure 3.13F). However, we could observed that in the non-irradiated controls xenografts the composition of

M1- and M2-like macrophages was highly heterogeneous ranging from ~16% to ~83% (coefficient of variation of "M1"=42.17%; "M2"=45.20%). Strikingly, upon radiation the ratios were less disperse, i.e. the M1-like percentage ranged from ~46% and ~64% and M2-like from ~35% to ~53% (coefficient of variation "M1"=13.49% and "M2"=17.84%), where the ratios became more similar between the different xenografts (Figure 3.13F).

Moreover, SHD-RT induced a reduction of 34% of other inflammatory cells besides macrophages (mpeg$^-$ tnfα$^+$, **P*=0.0350) (Figure 3.13F), being the neutrophils a strong candidate – since at this stage of zebrafish development macrophages and neutrophils are the main inflammatory cells (Renshaw and Trede, 2011).

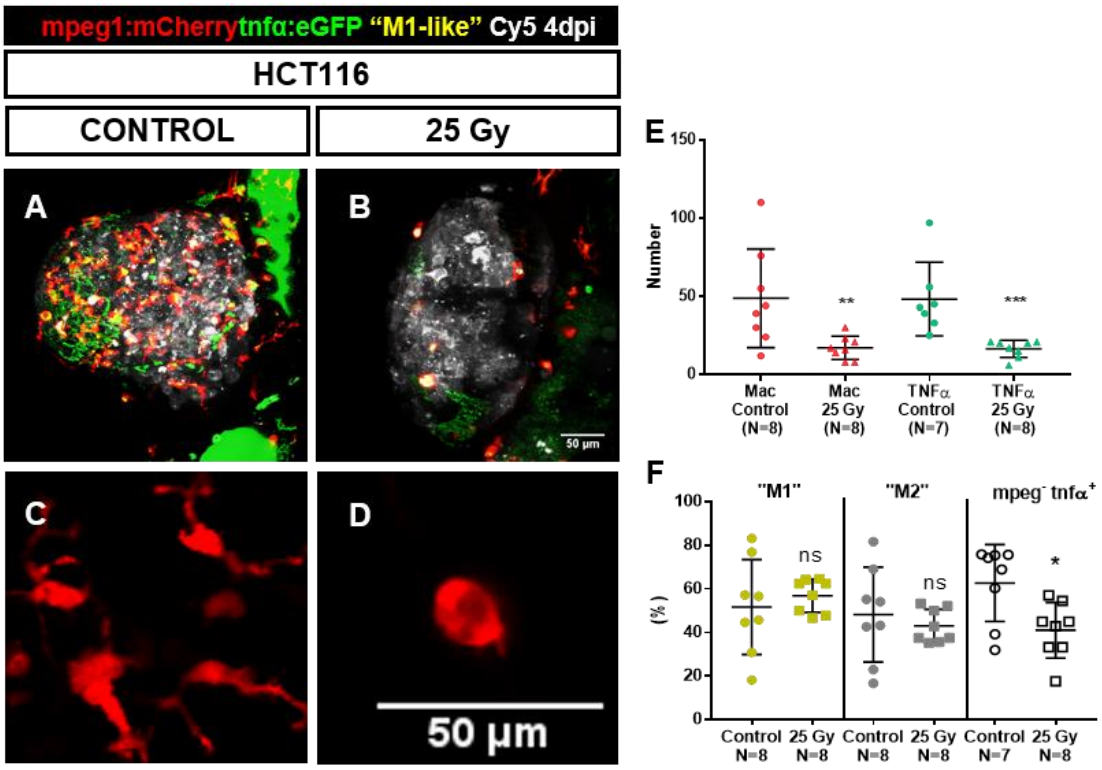

Figure 3.13. Radiation reduces both macrophages and inflammatory cell number. CRC xenografts were generated in a 2dpf mpeg1:mCherry tnfα:eGFP zebrafish, by HCT116 injection into the PVS. At 1dpi, xenografts were irradiated with SHD-RT (1x25Gy) and compared to the controls (non-irradiated xenografts). At 4dpi, both experimental conditions were analyzed in confocal microscopy and further quantifications were performed for: the total number of macrophages ("M1" and "M2") in red and the total TNFα factor in green (mpeg $^-$ tnfα$^+$ and mpeg$^+$tnfα$^+$) (E). Then the number of M1-like/M2-like and mpeg $^-$ tnfα$^+$ were divided by the total number of macrophages and the total number of inflammatory cells, respectively (F). Confocal microscopy images (A-D) were taken by a 25x objective. The total number of xenografts analyzed are indicated in E and F, where each dot represents an individual zebrafish xenograft. In E and F graphics were analyzed by Mann-Whitney test. *P values* **P*<0.05; ***P*<0.01; ****P*<0.001; ns, nonsignificant. Scale bar (50µm).

Moreover, during the quantifications of macrophages, it was observed a tendency of larger macrophages upon radiation compared to the non-irradiated macrophages, and also a high heterogeneity in macrophages morphology, showing a mixture of stellated (dendritic) and rounded shapes (Figure 3.13C and D). Thus, in order to further evaluate the radiation effect in macrophage morphology different phenotypic parameters' were investigated: macrophage area, perimeter and circularity. Interestingly, macrophages (M1-like and M2-like) dimensions increased upon RT (1 fold increase, *****P*<0.0001)

(Figure 3.14A), similar to HCT116 nuclear area size increase. Moreover morphology might be indicative of function/polarization of these cells towards a specific phenotype (M1-like or M2-like), in response to the interactions with TME (McWhorter *et al*., 2013; McWhorter *et al*., 2014) and to radiation (Genard *et al*., 2017). However, no differences were observed between M1-like and M2-like morphologies of the non-irradiated xenografts, prevailing a high morphologic heterogeneity in both. Despite the macrophages shapes heterogeneity, a slight increase of rounded M1-macrophages was observed (**P*=0.0285), following radiation (1.0 values indicate perfectly rounded macrophages, whereas values closer to 0.0 represent stellated shapes) (Figure3.14B).

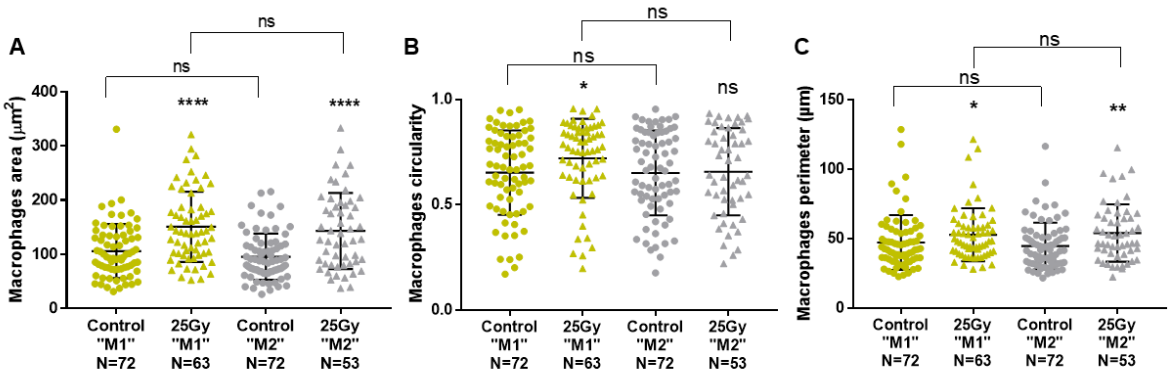

Figure 3.14. M1- and M2-like exhibit high heterogeneity in morphology. Macrophages morphology was analyzed according to the area (µm^2) (A), circularity (1.0 indicates perfect circles) (B) and perimeter (µm) (C). Each dot indicates an individual macrophage, where approximately 10 macrophages per xenograft were analyzed. *P values*: **P*<0.05;****P*<0.001 and *****P*<0.0001. Mann-Whitney test was applied.

In summary, our preliminary data showed that RT (1x25Gy) induces zebrafish innate immune suppression by decreasing the overall number of macrophages and suggested to reduce the variability of the ratios of M1- and M2-like macrophages in the TME, despite the non-statistical significance observed. Radiation also showed to elicit morphological changes in macrophages and also an overall reduction of the pro-inflammatory cells (tnfa$^+$ cells).

4. Discussion

Zebrafish have been recently shown to be a promising cancer avatar for personalized treatment, namely to screen Chemotherapy CRC tumor responses (Fior *et al*., 2017). Further, in order to develop the zebrafish model as a screening platform towards cancer personalized medicine, other therapies have to be tested, namely Radiotherapy (RT). Previous studies in the Lab tested the Neoadjuvant (NA) RT, a recommended treatment for rectal cancer (Glynne-Jones *et al*., 2017), in CRC zebrafish xenografts, revealing that is possible to distinguish different radiosensitivities (Póvoa and Fior, unpublished results). For logistical and executable reasons the RT regimen used was adapted based on the total irradiation dose given in the clinic (Fractionated RT - FRT, 5x5Gy), irradiating the CRC xenografts with a single dose of 25Gy (Single-High Dose RT – SHD-RT, 1x25Gy). Nevertheless, to guarantee that the SHD-RT protocol can be a good surrogate of tumor response to RT and no biological response is missed, the main goal of this thesis was to compare both RT protocols: SHD-RT (1x25Gy) versus FRT (5x5Gy), used in the clinic.

4.1 Single-High Dose RT Vs Fractionated RT: time and cumulative fractions are crucial factors for a more effective tumor response

Our study showed that SHD-RT (1x25Gy) induces similar therapeutic effects to FRT (5x5Gy), in 6 days. Both protocols induced direct DNA damage, blocking proliferation, increasing the nuclei dimensions and cell death that, consequently led to a clear tumor reduction. However, the CRC-xenografts submitted to the SHD-RT exhibited higher induction of apoptosis compared to the FRT irradiated xenografts. This finding raised the question whether SHD-RT could be stronger than FRT or alternatively if time after the last treatment was influencing the impact on tumor response. In the literature we can find controversial data: i.e. some that suggest that SHD-RT can elicit a stronger effects than FRT (Horsman *et al*., 2006) and others that suggests that both protocols induce a similar impact in tumor downsizing to FRT (Vanpouille-Box *et al*., 2017). On the other hand, it has been described the relevance of time after RT, where time has been shown to be determinant for the responses rates (Glynne-Jones *et al*., 2017), and that time shortening after RT may compromise the therapeutic potential of the fractionated doses (FRT) (Cho *et al*., 1999). These different studies raised the question whether the overall time after treatment ending could influence the CRC xenografts responses to RT.

Thus, to test if "time matters" for tumor response, the same time following treatment ending was given for both RT protocols (3 days after RT). Our data revealed that time is determinant for the effect of the cumulative fractions (FRT), which suggested to be more effective in tumor size reduction and nuclei enlargement than the Single-High Dose. These results were consistent with the previous studies in which time after RT is mentioned to be crucial for the radiobiology of the fractionated doses. Rega *et al*., 2016 also demonstrated that longer intervals between NA FRT (5x5Gy) and surgery (4-8 weeks rather than 2 weeks) lead to a more significant tumor reduction, in rectal cancer.

Together these results suggests that the daily 5Gy fractions elicits a sequential damage in cancer cells, where more cells are injured by radiation. This stronger effect is thought to be related to the fact

that cells are more sensitive to radiation in specific phases of the cell cycle, namely G_2/M (Wedenberg *et al*., 2013). Therefore in the single dose, although stronger – it will mostly affect the percentage of cells that are in G_2/M in that snapshot of time – one single time. In contrast, the fractionated protocol, although not so strong, by delivering 5 "snapshots" will increase the probability of affecting more overall cells in the radiosensitive phase of the cell cycle.

Surprisingly, longer intervals after FRT (3dpT) also revealed that this protocol induced a stronger increase in nuclei size than SHD-RT (3dpT). This phenotype, suggested that FRT and SHD-RT may elicit distinct biologic mechanisms. One hypothesis is that FRT radiobiology might induce a senescent phenotype whereas SHD-RT apoptosis cell death. To test this hypothesis, a senescence associated β-galactosidase assay might be performed in both protocols in these conditions (3dpT). Curiously, Vanpouille-Box and colleagues reported in a xenograft mice study, that SHD-RT (1x30Gy) and FRT (3x8Gy) induced similar effects in tumor downsizing. However the overall time given after both RT was not the same (FRT: 16dpT and SHD-RT: 18dpT), raising the question whether the FRT could exhibit a stronger tumoral mass reduction compared to SHD-RT, if the same time after RT was given like in our setting.

Overall, our study suggests that the adapted SHD-RT (1x25Gy) protocol is a feasible and quick assay that allows to determine radiosensitive CRC tumors. Moreover, our work showed the possibility to assess tumor response to RT in only 6 days with similar results to the long term experiments in murine studies, where at least one month is needed to evaluate the effect of anti-cancer treatments in tumor progression (Vanpouille-Box *et al*., 2017), delaying the pre-clinical insight and patients do not have time to wait. Additionally to be a less-time consuming assay, zebrafish allowed to determine radiosensitivity in a small scale, in which only a small amount of sample is required to reveal response to RT. Thus, the zebrafish model revealed to be very promising and advantageous as a fast cancer avatar for CRC xenografts RT radiosensitivity.

Nevertheless, given that FRT showed to be more effective than SHD-RT, when more time was given after RT, we need to test tumor response of radioresistant xenografts for both RT protocols, to ensure that the tumor that shows a radioresistant phenotype in the adapted protocol (SHD-RT) is maintained in the FRT. Only after this evaluation it will be possible to be confident that indeed the SHD-RT can be used as a good proxy to determine radiosensitivity/radioresistance.

4.2 Radiation suppresses the zebrafish innate immune system

Besides the main goal of this Thesis, I was involved in helping in the generation of zPDX and also in applying for the first time the adapted RT protocol (SHD-RT, 1x25Gy) alone or in combination with Chemotherapy (FOLFOX). Our data showed that the example of rectum zPDX (zPDX#5) was more sensitive to the combinatorial treatment than to RT alone, suggesting an additive or synergism effect between both therapies. However, to confirm this the zPDX should have been also submitted to FOLFOX alone.

Curiously, we observed that most the rectum zPDX subjected to radiation suggested to have better implantation rates upon treatment, and showed an increase in the number of cells positive for human

mitochondria. Radiation is often used xenografts studies (mouse and adult zebrafish) to suppress its immune system in order to improve tumor establishment, avoiding rejection (Pompili *et al*., 2016, Glass *et al*., 2013). However, this ablation is mainly concerning the adaptive immune system. Thus, we tested whether radiation could also be affecting the innate immune system of zebrafish. Our data showed a significant reduction in the number of macrophages and other inflammatory cells. Therefore, our results are consistent with Filatenkov *et al*., 2015 study which demonstrated the capacity of a single ablative irradiation of 30Gy to reduce tumor-associated macrophages (TAMs) in mice.

Moreover we suspect that the other population of inflammatory cells ($mpeg^{-}$ $tnf\alpha^{+}$) that also reduced after RT might be neutrophils, since they are the other main innate player at this state of zebrafish development and have been shown to express TNFα (Renshaw and Trede, 2011; Tecchio *et al*., 2014). These results are also in agreement with the described neutropenia (low number of neutrophils) observed upon RT in patients (Manus *et al*., 1997).

In addition to the overall reduction of macrophage numbers we also analyzed their polarization. Intriguingly, we observed a redistribution of the ratios upon RT: in the non-irradiated controls a highly heterogeneous distribution of M1-like and M2-like was observed ranging from ~16% to ~83%, in clear contrast to the consistent ratios of 57% M1-like and 43% M2-like ratio upon radiation. Concomitantly with this, we also observed an increase of larger macrophages upon radiation. These results suggested that radiation may also induce direct effects in macrophages, similar to the observed in the nuclei of CRC cells after RT, increasing their morphological dimensions.

Genard *et al*., 2017, suggested that superior doses to 12Gy may lead to a M2-like polarization instead we observed a reduction of in the heterogeneity of phenotypes. It has been also suggested, in several studies, that the shape of macrophages may indicate a polarization towards a specific phenotype. However, we found contracting literature regarding the shape and function of macrophages i.e. we found studies claiming that M2-like macrophages are more associated with a stellate and dendritic shape whereas M1-like are more rounded but other studies claimed the opposite (McWhorter *et al*., 2013; McWhorter *et al*., 2014). Nevertheless, regarding our data and the pro-inflammatory factor (TNFα) used to distinguish M1-like from M2-like, it was not possible to correlate the macrophages morphology to the TNFα factor.

In summary, our results showed that in addition to the anti-tumoral therapeutic effects that radiation elicits, it can also suppress the zebrafish innate immune cells.

4.3 Conclusion

Overall, our work suggests that zebrafish model is a promising model that allows to assess tumor response to RT in a very short time. Our data showed that SHD-RT (1x25Gy) seems a suitable, feasible and quick RT protocol that enables to determine radiosensitivity of CRC, in only six days. However, when compared to the radiobiology of FRT (5x5Gy, given in the clinic), with the same overall time after treatment ending, the FRT revealed to be more effective than the SHD-RT. Thus, cumulative damage and time are crucial factors for an effective tumor response.

We also showed that besides the anti-cancer therapeutic effects of RT, radiation also seems to induce a suppressive effect on macrophages and inflammatory cell numbers. Despite the published data regarding the impact of Single-High Doses in macrophages phenotype modulation towards a M2-like profile, no significant differences were observed in the M1- and M2-like rates after SHD-RT compared to the non-irradiated controls. Nevertheless, RT was able to modify the macrophages morphology, to larger and rounded M1-like macrophages, however no correlation between shape and function was observed.

In summary, our study showed the potential of zebrafish model to investigate cancer biology in response to RT. Hopefully, we expect that it will be possible to screen patients to the recommended therapies, aiming a fast and feasible cancer avatar for personalized medicine, to help clinical treatment decisions. Thus, if its predictability stands, this personalized platform may guide therapy for each patient, concerning its unique and specific cancer profile, avoiding unnecessary toxicities.

4.4 Future work

Since FRT (5x5Gy) revealed to be more effective than SHD-RT, it is essential to further test the response of radioresistant xenografts, to guarantee that the SHD-RT is indeed an appropriate protocol to distinguish radiosensitivity from radioresistance. Thus, radioresistant CRC xenografts (e.g. Hke3) have to be generated in 2dpf zebrafish, and then randomly divided into the three experimental conditions: Control (non-irradiated xenografts); FRT (5x5Gy); and SHD-RT (1x25Gy) and given the same interval of time after treatment ending for both RT regimens (3dpT). We expect that both RT regimens will act similarly in the resistant xenografts, i.e. induce little or no effect on apoptosis and tumor size reduction.

It would be also interesting to investigate if FRT and SHD-RT therapeutic effects have distinct biologic mechanisms, since we could observe in the FRT a marked increase in nuclei size, compared to SHD-RT given the same overall time after treatment - this maybe suggestive of an induction of senescence. To address this question we can perform a β-galactosidase assay in the HCT116-CRC xenografts after 3dpT (conditions of experiment of Figure 3.4A).

Our results showed that radiation (1x25Gy) suppresses macrophages and other inflammatory cells, possibly neutrophils. Thus, to better understand whether radiation can influence neutrophils and its behavior after treatment it could be interesting to test SHD-RT and FRT in zebrafish xenografts, using the Mpx transgenic (which labels neutrophils). Moreover, it could be also very interesting to evaluate the differential effect of RT regimens (SHD-RT and FRT) in macrophages phenotype and whether the communication between cancer cells and macrophages can influence tumor response to RT, testing in different types of tumors, using zebrafish as the *in vivo* model.

Finally, and most importantly zebrafish predictability to assess tumor responses to RT needs to be tested suing biopsy patients of rectal patients that will be subjected to NA RT. Correlations between the patient response to NA therapy (accessed by imaging, surgery and pathology of the surgical specimen) with the induction of apoptosis in the matching zPDX. We expect that will be possible to correlate higher induction of apoptosis with patients that had a good response to therapy.

5. Appendix

5.1 Materials

The following materials were prepared by the Champalimaud Fish Facility:

Table 5.1. List of embryo medium components

Embryo medium (E3)	
50x E3 – stock For 10 L of Milli-Q water (sterile)	**1x E3 – ready to use**
146,9g NaCl	400mL 50x E3
6,3g KCl	60mL 0.01% Methylene Blue Solution (0,05g Methylene Blue powder in 500 mL Milli-Q water)
24,3g $CaCl_2.2H_2O$	Fill to 20L with system water
40,7g $MgSO_4.7H_2O$	

Table 5.2. List of pronase components

Pronase	
100x Pronase (60 mg/mL) – stock	**1x Pronase (0.6 mg/mL) – ready to use**
1g Pronase (Roche)	dilute 100µL 100x pronase stock solution in 9.9mL 1x Embryo Medium (E3) without methylene blue
16,7mL MQ water	aliquot to 500µL
aliquot to 100µL	

Table 5.3. List of Tricaine components

Tricaine	
25x Tricaine (60mg/mL) – stock and euthanasia	**1x Tricaine – anesthesia**
2g Tricaine powder	dilute 20mL 25x Tricaine in 480mL system water
500mL reverse osmosis (RO) water	
10mL 1M Tris (pH 9) (1M Tris: 121.14g Trizma base in 1L RO water)	
adjust pH ~7	

Table 5.4. Reagents and solutions for CRC patient samples processing (adapted from Fior *et al*., 2017)

	Reagent	Description (Reference)	Supplier	Final concentration
Collection medium	Advanced DMEM/F-12	Cell culture medium (Arora, 2013)	Gibco	-
	Penicillin-Streptomycin	Antibiotic to prevent bacterial contamination (against gram positive and negative bacteria) (Ryu *et al*., 2017)	Sigma-Aldrich	100U/mL
	Amphotericin B solution	Antifugical antibiotic (Khun *et al*., 2002)	Sigma-Aldrich	100µg/mL
	Kanamycin solution	Aminoglycoside bacteriocidal antibiotic (Kohanski *et al*., 2007)	Sigma-Aldrich	100µg/mL
	Gentamicin solution	Aminoglycoside bacteriocidal antibiotic (Davis *et al*., 1986)	Sigma-Aldrich	500µg/mL
	Nystatin Suspension	Antifungical (Kuhn *et al*., 2002)	Sigma-Aldrich	2400U/mL
	Amoxicillin/Clavulanic acid	Antibiotic against bacteria (Adam *et al*., 1982)	Clavepen	220µg/mL
	Metronidazole	Antibiotic against bacteria or parasites (Ghannoum and Rice, 1999)	Braun	80µg/mL
Mix 1	Roswell Park Memorial Institute medium (RPMI) or DMEM F12 + HEPES+ Glutamine	Cell culture medium (Arora, 2013)	Gibco	1% HEPES and 1% Glutamine
	FBS (fetal bovine serum)	Growth supplement with high content of embryonic growth promoting factors (Arora, 2013)	Gibco	60%
	Primocin	Antibiotic against mycoplasma, bacterial and fungi contaminations (Bartfeld *et al*., 2015)	Invivogen	100µg/mL
	Anoikis inhibitor	Inhibition of anoikis, a programmed cell death induced by the cell detachment from extracellular matrix (Frisch and Screaton, 2001)	Sigma-Aldrich	10µM
	Putrescine	Important polyamine in cell cycle (Martin, 1991)	Sigma-Aldrich	10µg/mL
	p38 inhibitor	Inhibition of p38, mitogen activated protein kinase (MAPKs) associated in inflammation (Kummer *et al*., 1997)	Sigma-Aldrich	10µM
	Nicotinamide	Coenzyme precursor NAD^+ important in cell survival (Hsu *et al*., 2009)	Sigma-Aldrich	10mM
Mix 2	DPBS	Equilibrated salt solution with several functions, such as washing cells before digestion (Arora, 2013)	Gibco	1x

	Glucose	Carbohydrate (sugar) as energy source (Arora, 2013)	Sigma-Aldrich	0.2%
	Primocin	Antiobiotic against mycoplasma, bacterial and fungi contaminations (Bartfeld *et al*., 2015)	Invivogen	100µg/mL
	Anoikis inhibitor	Inhibition of anoikis, a programmed cell death induced by the cell detachment from extracellular matrix (Frisch and Screaton, 2001).	Sigma-Aldrich	10µM
	Putrescin	Important polyamine in cell cycle (Martin, 1991)	Sigma-Aldrich	10µg/mL
	Glutamine	Important aminoacid for cell proliferation (protein synthesis) (Arora, 2013)	ThermoFisher Scientific	1%
	Nicotinamide	Coenzyme precursor NAD^+ important in cell survival (Hsu *et al*., 2009)	Sigma-Aldrich	10mM
	Epidermal Growth Factor (EGF)	Small polypeptide involved in cell signaling pathways that promote cell proliferation (Bettger *et al*., 1981)	PeproTech	50ng/mL
	Fibroblast Growth Factor (FGF)	Important in signaling pathways associated with cell proliferation, migration, differentiation and angiogenesis (Korc and Friesel, 2009)	PeproTech	100ng/mL
	Ethylenediaminetetraacetic acid (EDTA)	Chelating agent for cells detachment (Okano T. *et al.*,1995)	Sigma	2mM
	Insulin	Growth factor for cell proliferation (Strange *et al*., 2004)	Sigma-Aldrich	10µg/mL
	Vybrant CM-DiI	Lipophilic dye (Andrade W. *et al.*, 1996)	Molecular Probes, Life Technologies	4µL/mL
Mix 3 (980 µL Mix1)	Epidermal Growth Factor (EGF)	Small polypeptide involved in cell signaling pathways that promote cell proliferation (Bettger *et al*., 1981)	PeproTech	50ng/mL
	Fibroblast Growth Factor (FGF)	Important in signaling pathways associated with cell proliferation, migration, differentiation and angiogenesis (Korc and Friesel, 2009)	PeproTech	100ng/mL
	Glutamine	Important aminoacid for cell proliferation (protein synthesis) (Arora, 2013)	ThermoFisher Scientific	1%
	Insulin	Growth factor for cell proliferation (Strange *et al*., 2004)	Sigma-Aldrich	10µg/mL

Table 5.5. CRC standard Chemotherapy components, description of its mode of action, final concentration and patient plasma concentration (adapted from Fior *et al.*, 2017)

Chemotherapy compounds	Mode of action	Final concentration (mM)	Patient plasma concentration (nM)
5-FU	Fluoropyrimidine blocks thymidylic acid formation; DNA biosynthesis (Longley *et al.*, 2003)	4.2	426.46
Oxaliplatin	DNA crossliking agent; preventing DNA replication and transcription (Seetharam *et al.*, 2010)	0.08	8.1
Folinic acid or leucoverin	Stabilizes binding of 5-FU to thymidylate synthase (Erlichman *et al.*, 1988)	0.18	18.5

5.2 Results

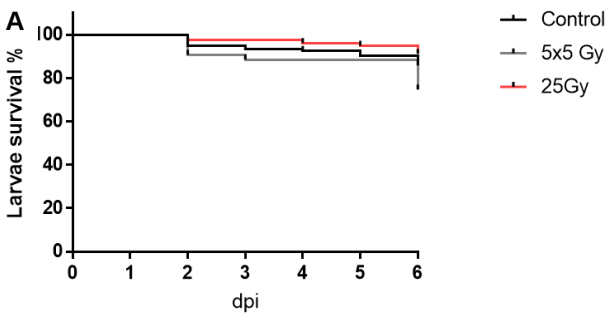

Figure 5.1. Zebrafish survival of the three experimental conditions (Control, 5x5Gy and 1x25Gy), until 6 dpi. The Kaplan-Meier curve indicates the larvae survival percentage of two independent experiments. Chi-square was the statistical analysis performed. The 5x5Gy regimen was the condition with higher mortality percentage (25%) compared to the Control (14.19% death, **P*<0.05) and to the 1x25Gy (8% death, ***P*<0.01).

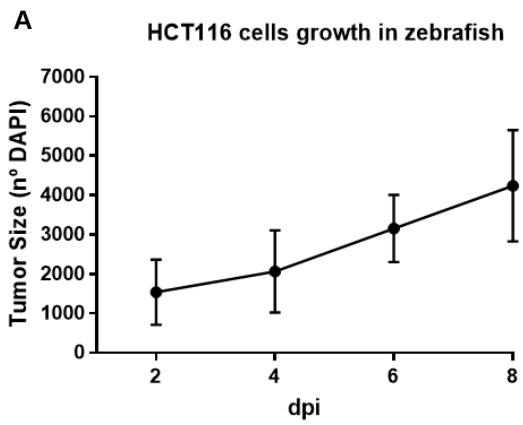

Figure 5.2. Growth rate of CRC HCT116 cells in zebrafish. The values in A are the overall results obtained from the quantification of the tumor size from all non-irradiated controls xenografts along the RT experiments. Thus, it was possible to analyze HCT116 cells proliferation in zebrafish through time. Regarding the DAPI numbers, HCT116 showed to double the size in 4 days: 2dpi AVG=1538,74; 4dpi AVG=2059,53; 6dpi AVG= 3151,34; 8dpi AVG=4239,08. For the results in Figure 3.8 it was estimated that the tumor size at 5dpi had an average of ~ 2900 cells. Given that HCT116 cells doubled de size in 4 days, it was estimated that at 1dpi the tumor size should exhibited an average of ~1450 cells, i.e. from day 1 to day 5, the CRC cells increased the double.

6. References

Adam, D. *et al*., (1982). Pharmacokinetics of amoxicillin and clavulanic acid administered alone and in combination. *Antimicrobial Agents and Chemotherapy*, 22(3), pp.353-357.

Alberts, B. *et al*., (2002). *Molecular biology of the cell*. 4th ed. NY: Garland Science.

Anari, F. *et al*., (2018). Impact of tumor microenvironment composition on therapeutic responses and clinical outcomes in cancer. *Future Oncology*, 14(14), pp.1409-1421.

Andrade, W. *et al*., (1996). The use of the lipophilic fluorochrome CM-DiI for tracking the migration of lymphocytes. *Journal of Immunological Methods*, 194(2), pp.181-189.

Arora, M. (2013). *Cell Culture Media: A Review*. Materials and Methods, 3, p.175.

Astone, M. *et al*., (2017). Fishing for cures: The alLURE of using zebrafish to develop precision oncology therapies. *npj Precision Oncology*, 1(1), p.39.

Balkwill, F. *et al*., (2012). The tumor microenvironment at a glance. *Journal of Cell Science*, 125(23), pp.5591-5596.

Barcellos-Hoff, M. *et al*., (2005). Radiation and the microenvironment – tumorigenesis and therapy. *Nature Reviews Cancer*, 5(11), pp.867-875.

Bartfeld, S. *et al*., (2015). In Vitro Expansion of Human Gastric Epithelial Stem Cells and Their Responses to Bacterial Infection. *Gastroenterology*, 148(1), pp.126-136.e6.

Barriuso, J. *et al*., (2015). Zebrafish: A New Companion for Translational Research in Oncology. *Clinical Cancer Research*, 21(5), pp.969-975.

Baskar, R. *et al*., (2012). Cancer and Radiation Therapy: Current Advances and Future Directions. *International Journal of Medical Sciences*, 9(3), pp.193-199.

Baskar, R. *et al*., (2014). Biological response of cancer cells to radiation treatment. *Frontiers in Molecular Biosciences*, 1, p.24.

Bentley, V. *et al*., (2015). Focused chemical genomics using zebrafish xenotransplantation as a pre-clinical therapeutic platform for T-cell acute lymphoblastic leukemia. *Haematologica*, 100(1), pp.70-76.

Bernut, A. *et al*., (2016). Mycobacterium abscessus-Induced Granuloma Formation Is Strictly Dependent on TNF Signaling and Neutrophil Trafficking. *PLOS Pathogens*, 12(11), p.e1005986.

Bettger, W. *et al*., (1981). Rapid clonal growth and serial passage of human diploid fibroblasts in a lipid-enriched synthetic medium supplemented with epidermal growth factor, insulin, and dexamethasone. *Proceedings of the National Academy of Sciences*, 78(9), pp.5588-5592.

Briffa, R., *et al*., (2018). Acquired and intrinsic resistance to colorectal cancer treatment. In J. Chen (Ed.), *Colorectal Cancer: Diagnosis, Screening and Management* InTech.

Brown, J. and Koong, A. (2008). High-Dose Single-Fraction Radiotherapy: Exploiting a New Biology?. *International Journal of Radiation Oncology*Biology*Physics*, 71(2), pp.324-325.

Brown, J. *et al*., (2010). Stereotactic Ablative Radiotherapy Should Be Combined With a Hypoxic Cell Radiosensitizer. *International Journal of Radiation Oncology*Biology*Physics*, 78(2), pp.323-327.

Burrell, R. *et al*., (2013). The causes and consequences of genetic heterogeneity in cancer evolution. *Nature*, 501(7467), pp.338-345.

Byrne, A. *et al*., (2017). Interrogating open issues in cancer precision medicine with patient-derived xenografts. *Nature Reviews Cancer*, 17(4), pp.254-268.

Castedo, M. *et al*., (2004). Cell death by mitotic catastrophe: a molecular definition. *Oncogene*, 23(16), pp.2825-2837.

Cho, K. *et al*., (1999). Single dose versus fractionated stereotactic radiotherapy for recurrent high-grade gliomas. *International Journal of Radiation Oncology*Biology*Physics*, 45(5), pp.1133-1141.

Collado, M. and Serrano, M. (2006). The power and the promise of oncogene-induced senescence markers. *Nature Reviews Cancer*, 6(6), pp.472-476.

Cutsem, V. *et al*., (2016). ESMO consensus guidelines for the management of patients with metastatic colorectal cancer. *Annals of Oncology*, 27(8), pp.1386-1422.

Dagogo-Jack, I. and Shaw, A. (2017). Tumour heterogeneity and resistance to cancer therapies. *Nature Reviews Clinical Oncology*, 15(2), pp.81-94.

Davis, B. *et al*., (1986). Misread protein creates membrane channels: an essential step in the bactericidal action of aminoglycosides. *Proceedings of the National Academy of Sciences*, 83(16), pp.6164-6168.

Dayde, D. *et al*., (2017). Predictive and Prognostic Molecular Biomarkers for Response to Neoadjuvant Chemoradiation in Rectal Cancer. *International Journal of Molecular Sciences*, 18(3), p.573.

De Felice, F. *et al*., (2017). The role of radiation therapy in bone metastases management. *Oncotarget*, 8(15), pp. 25691–25699.

Deloch, L. *et al*., (2016). Modern Radiotherapy Concepts and the Impact of Radiation on Immune Activation. *Frontiers in Oncology*, 6, p.141.

Dewan, M. *et al*., (2009). Fractionated but Not Single-Dose Radiotherapy Induces an Immune-Mediated Abscopal Effect when Combined with Anti-CTLA-4 Antibody. *Clinical Cancer Research*, 15(17), pp.5379-5388.

Elgazzar, A. (2006). *The pathophysiologic basis of nuclear medicine*. 2nd ed. Berlin: Springer.

Erlichman, C. *et al*., (1988). A randomized trial of fluorouracil and folinic acid in patients with metastatic colorectal carcinoma. *Journal of Clinical Oncology*, 6(3), pp.469-475.

Ellett, F. *et al*., (2010). mpeg1 promoter transgenes direct macrophage-lineage expression in zebrafish. *Blood*, 117(4), pp.e49-e56.

Filatenkov, A. *et al*., (2015). Ablative Tumor Radiation Can Change the Tumor Immune Cell Microenvironment to Induce Durable Complete Remissions. *Clinical Cancer Research*, 21(16), pp.3727-3739.

Fior, R. *et al*., (2017). Single-cell functional and chemosensitive profiling of combinatorial colorectal therapy in zebrafish xenografts. *Proceedings of the National Academy of Sciences*, 114(39), pp.E8234-E8243.

Folkert, M. and Timmerman, R. (2017). Stereotactic ablative body radiosurgery (SABR) or Stereotactic body radiation therapy (SBRT). *Advanced Drug Delivery Reviews*, 109, pp.3-14.

Frisch, S. and Screaton, R. (2001). Anoikis mechanisms. *Current Opinion in Cell Biology*, 13(5), pp.555-562.

Gash, K. *et al*., (2017). Factors associated with degree of tumour response to neo-adjuvant radiotherapy in rectal cancer and subsequent corresponding outcomes. *European Journal of Surgical Oncology*, 43(11), pp.2052-2059.

Gasinska, A. *et al*., (2004). Influence of overall treatment time and radiobiological parameters on biologically effective doses in cervical cancer patients treated with radiation therapy alone. *Acta Oncologica*, 43(7), pp.657-666.

Geiger, G. *et al*., (2008). Temozolomide-Mediated Radiosensitization of Human Glioma Cells in a Zebrafish Embryonic System. *Cancer Research*, 68(9), pp.3396-3404.

Genard, G. *et al*., (2017). Reprogramming of Tumor-Associated Macrophages with Anticancer Therapies: Radiotherapy versus Chemo- and Immunotherapies. *Frontiers in Immunology*, 8, p.828.

Ghannoum, M. and Rice, L. (1999). Antifungal Agents: Mode of Action, Mechanisms of Resistance, and Correlation of These Mechanisms with Bacterial Resistance. *Clinical Microbiology Reviews*, 12(4), pp.501–517.

Glass, T. *et al*., (2013). Effect of Radiation Dose-Rate on Hematopoietic Cell Engraftment in Adult Zebrafish. *PLoS ONE*, 8(9), p.e73745.

Glynne-Jones, R. *et al*., (2017). Rectal cancer: ESMO Clinical Practice Guidelines for diagnosis, treatment and follow-up. *Annals of Oncology*, 28(suppl_4), pp.iv22-iv40.

Goldstein, M. and Kastan, M. (2015). The DNA Damage Response: Implications for Tumor Responses to Radiation and Chemotherapy. *Annual Review of Medicine*, 66(1), pp.129-143.

Guedea, M. *et al.*, (2013). Single high-dose vs. fractionated radiotherapy: Effects on plant growth rates. *Reports of Practical Oncology & Radiotherapy*, 18(5), pp.279-285.

Haldi, M. *et al*., (2006). Human melanoma cells transplanted into zebrafish proliferate, migrate, produce melanin, form masses and stimulate angiogenesis in zebrafish. *Angiogenesis*, 9(3), pp.139-151.

Hanahan, D. and Weinberg, R. (2011). Hallmarks of Cancer: The Next Generation. *Cell*, 144(5), pp.646-674.

Hellevik, T. and Martinez-Zubiaurre, I. (2014). Radiotherapy and the Tumor Stroma: The Importance of Dose and Fractionation. *Frontiers in Oncology*, 4, p.1.

Hof, H. *et al*., (2003). Stereotactic single-dose radiotherapy of stage I non–small-cell lung cancer (NSCLC). *International Journal of Radiation Oncology*Biology*Physics*, 56(2), pp.335-341.

Horsman, M. *et al*., (2006). Radiation administered as a large single dose or in a fractionated schedule: Role of the tumour vasculature as a target for influencing response. *Acta Oncologica*, 45(7), pp.876-880.

Hoskin, P. *et al*., (2017). SCORAD III: Randomized noninferiority phase III trial of single-dose radiotherapy (RT) compared to multifraction RT in patients (pts) with metastatic spinal canal compression (SCC). *Journal of Clinical Oncology*, 35(18_suppl), pp.LBA10004-LBA10004.

Hsu, C. *et al*., (2009). Nicotinamide Phosphoribosyltransferase Regulates Cell Survival Through NAD+Synthesis in Cardiac Myocytes. *Circulation Research*, 105(5), pp.481-491.

Kim, N., *et al*., (2017). Serum CEA and CA 19-9 Levels are Associated with the Presence and Severity of Colorectal Neoplasia. *Yonsei Medical Journal*, 58(5), p.918.

Kirchberger, S. *et al*., (2017). Quo natas, Danio?—Recent Progress in Modeling Cancer in Zebrafish. *Frontiers in Oncology*, 7, p.186.

Klement, R. (2017). The influence of ketogenic therapy on the 5 R's of radiobiology. *International Journal of Radiation Biology*, 9, pp.1-13.

Klemm, F. and Joyce, J. (2015). Microenvironmental regulation of therapeutic response in cancer. *Trends in Cell Biology*, 25(4), pp.198-213.

Kuipers, E. *et al*., (2015). Colorectal cancer. *Nature Reviews Disease Primers*, 1, p.15065.

Kohanski, M. *et al*., (2007). A Common Mechanism of Cellular Death Induced by Bactericidal Antibiotics. *Cell*, 130(5), pp.797-810.

Korc, M. and Friesel, R. (2009). The Role of Fibroblast Growth Factors in Tumor Growth. *Current Cancer Drug Targets*, 9(5), pp.639-651.

Kuhn, D. *et al*., (2002). Antifungal Susceptibility of Candida Biofilms: Unique Efficacy of Amphotericin B Lipid Formulations and Echinocandins. *Antimicrobial Agents and Chemotherapy*, 46(6), pp.1773-1780.

Kummer, J. *et al*., (1997). Apoptosis Induced by Withdrawal of Trophic Factors Is Mediated by p38 Mitogen-activated Protein Kinase. *Journal of Biological Chemistry*, 272(33), pp.20490-20494.

Lai, Y. *et al*., (2017). Current status and perspectives of patient-derived xenograft models in cancer research. *Journal of Hematology & Oncology*, 10(1), p.106.

Lally, B. *et al*., (2007). Identification and Biological Evaluation of a Novel and Potent Small Molecule Radiation Sensitizer via an Unbiased Screen of a Chemical Library. *Cancer Research*, 67(18), pp.8791-8799.

Lawson, N. and Weinstein, B. (2002). In Vivo Imaging of Embryonic Vascular Development Using Transgenic Zebrafish. *Developmental Biology*, 248(2), pp.307-318.

Lee, L. *et al*., (2005). The fate of human malignant melanoma cells transplanted into zebrafish embryos: Assessment of migration and cell division in the absence of tumor formation. *Developmental Dynamics*, 233(4), pp.1560-1570.

Leksell L. (1951). The stereotaxic method and radiosurgery of the brain. *Acta Chir Scand*. 102, pp.316-9.

Liu, S. and Leach, S. (2011). Zebrafish Models for Cancer. *Annual Review of Pathology: Mechanisms of Disease*, 6(1), pp.71-93.

Longley, D. *et al*., (2003). 5-Fluorouracil: mechanisms of action and clinical strategies. *Nature Reviews Cancer*, 3(5), pp.330-338.

Maier, P. *et al*., (2016). Cellular Pathways in Response to Ionizing Radiation and Their Targetability for Tumor Radiosensitization. *International Journal of Molecular Sciences*, 17(1), p.102.

Manus, M. *et al*., (1997). Radiotherapy-Associated Neutropenia and Thrombocytopenia: Analysis of Risk Factors and Development of a Predictive Model. *Blood*, 89, pp.2303-2310.

Marques, I. *et al*., (2009). Metastatic behaviour of primary human tumours in a zebrafish xenotransplantation model. *BMC Cancer*, 9(1), p.128.

Martin, R. (1991). Cell cycle-dependent uptake of putrescine and its importance in regulating cell cycle phase transition in cultured adult mouse hepatocytes. *Hepatology*, 14(6), pp.1243-1250.

Matchett, K. *et al*., (2017). Advances in Precision Medicine: Tailoring Individualized Therapies. *Cancers*, 9(12), p.146.

McWhorter, F. *et al*., (2013). Modulation of macrophage phenotype by cell shape. *Proceedings of the National Academy of Sciences*, 110(43), pp.17253-17258.

McWhorter, F. *et al.*, (2014). Physical and mechanical regulation of macrophage phenotype and function. *Cellular and Molecular Life Sciences*, 72(7), pp.1303-1316.

Mercatali, L. *et al*., (2016). Development of a Patient-Derived Xenograft (PDX) of Breast Cancer Bone Metastasis in a Zebrafish Model. *International Journal of Molecular Sciences*, 17(8), p.1375.

Nagle, P. *et al*., (2018). Patient-derived tumor organoids for prediction of cancer treatment response. *Seminars in Cancer Biology*, 53, pp.258-264.

Nyman, J. *et al*., (2016). SPACE – A randomized study of SBRT vs conventional fractionated radiotherapy in medically inoperable stage I NSCLC. *Radiotherapy and Oncology*, 121(1), pp.1-8.

Okano, T. *et al*., (1995). Mechanism of cell detachment from temperature-modulated, hydrophilic-hydrophobic polymer surfaces. *Biomaterials*, 16(4), pp.297-303.

Okuyama, T. *et al*., (2018). Therapeutic effects of oxaliplatin-based neoadjuvant chemotherapy and chemoradiotherapy in patients with locally advanced rectal cancer: a single-center, retrospective cohort study. *World Journal of Surgical Oncology*, 16(1), p.105.

Peri, F. and Nüsslein-Volhard, C. (2008). Live Imaging of Neuronal Degradation by Microglia Reveals a Role for v0-ATPase a1 in Phagosomal Fusion In Vivo. *Cell*, 133(5), pp.916-927.

Pinto, A. *et al*., (2016). Intricate Macrophage-Colorectal Cancer Cell Communication in Response to Radiation. *PLOS ONE*, 11(8), p.e0160891.

Pompili, L. *et al*., (2016). Patient-derived xenografts: a relevant preclinical model for drug development. *Journal of Experimental & Clinical Cancer Research*, 35(1), p.189.

Pouliliou, S. and Koukourakis, M. (2014). Gamma histone 2AX (γ-H2AX) as a predictive tool in radiation oncology. *Biomarkers*, 19(3), pp.167-180.

Renshaw, S. *et al*., (2006). A transgenic zebrafish model of neutrophilic inflammation. *Blood*, 108(13), pp.3976-3978.

Renshaw, S. and Trede, N. (2011). A model 450 million years in the making: zebrafish and vertebrate immunity. *Disease Models & Mechanisms*, 5(1), pp.38-47.

Ryu, A. *et al*., (2017). Use antibiotics in cell culture with caution: genome-wide identification of antibiotic-induced changes in gene expression and regulation. *Scientific Reports*, 7(1), p.7533.

Seetharam, R. *et al*., (2010). Oxaliplatin: Preclinical perspectives on the mechanisms of action, response and resistance. *ecancermedicalscience*, 3, p.153.

Stakheyeva, M. *et al*., (2017). Role of the immune component of tumor microenvironment in the efficiency of cancer treatment: perspectives for the personalized therapy. *Current Pharmaceutical Design*, 23(32), pp. 4807-4826.

Stiksma, J. *et al*., (2014). CA 19-9 As a Marker in Addition to CEA to Monitor Colorectal Cancer. *Clinical Colorectal Cancer*, 13(4), pp.239-244.

Stokes, W. *et al*., (2017). Implementation of hypofractionated prostate radiation therapy in the United States: A National Cancer Database analysis. *Practical Radiation Oncology*, 7(4), pp.270-278.

Strange, K. *et al*.,(2004). Mitogenic Properties of Insulin-Like Growth Factors I and II, Insulin-like Growth Factor Binding Protein-3 and Epidermal Growth Factor on Human Breast Stromal Cells in Primary Culture. *Breast Cancer Research and Treatment*, 84(2), pp.77-84.

Taylor, A. and Zon, L. (2009). Zebrafish Tumor Assays: The State of Transplantation. *Zebrafish*, 6(4), pp.339-346.

Tecchio, C. *et al*., (2014). Neutrophil-Derived Cytokines: Facts Beyond Expression. *Frontiers in Immunology*, 5, p.508.

Teng, Y. *et al*., (2013). Evaluating human cancer cell metastasis in zebrafish. *BMC Cancer*, 13(1), p.453.

Tian, Y. *et al*., (2017). The first wave of T lymphopoiesis in zebrafish arises from aorta endothelium independent of hematopoietic stem cells. *The Journal of Experimental Medicine*, 214(11), pp.3347-3360.

Todde, V. *et al*., (2009). Autophagy: Principles and significance in health and disease. *Biochimica et Biophysica Acta (BBA) - Molecular Basis of Disease*, 1792(1), pp.3-13.

Twelves, C. *et al*., (2005). Capecitabine as Adjuvant Treatment for Stage III Colon Cancer. *New England Journal of Medicine*, 352(26), pp.2696-2704.

Vanpouille-Box, C. *et al*., (2017). DNA exonuclease Trex1 regulates radiotherapy-induced tumour immunogenicity. *Nature Communications*, 8, p.15618.

Wang, J. *et al*., (2018). Biological effects of radiation on cancer cells. *Military Medical Research*, 5(1).

Wedenberg, M. (2013). *From cell survival to dose response: modeling biological effects in radiation therapy*. Department of Oncology-Pathology. Karolinska Institutet, Stockholm, Sweden.

Weichselbaum, R. *et al*., (2017). Radiotherapy and immunotherapy: a beneficial liaison?. *Nature Reviews Clinical Oncology*, 14(6), pp.365-379.

White, R. *et al*., (2008). Transparent Adult Zebrafish as a Tool for In Vivo Transplantation Analysis. *Cell Stem Cell*, 2(2), pp.183-189.

Williams, J. (2018). Using PDX for Preclinical Cancer Drug Discovery: The Evolving Field. *Journal of Clinical Medicine*, 7(3), p.41.

Wistuba, I. *et al*., (2011). Methodological and practical challenges for personalized cancer therapies. *Nature Reviews Clinical Oncology*, 8(3), pp.135-141.

Wu, D. *et al*., (2017a). Network meta-analysis of the efficacy of first-line chemotherapy regimens in patients with advanced colorectal cancer. *Oncotarget*, 8(59), pp. 100668–100677.

Wu, J. *et al*., (2017b). Patient-derived xenograft in zebrafish embryos: a new platform for translational research in gastric cancer. *Journal of Experimental & Clinical Cancer Research*, 36(1), p.160.

Xiao, Y. *et al*., (2016). Deficiency of 53BP1 inhibits the radiosensitivity of colorectal cancer. *International Journal of Oncology*, 49(4), pp.1600-160.